JGR Earth Surface

RESEARCH ARTICLE
10.1029/2021JF006537

Influence of Rarely Mobile Boulders on Channel Width and Slope: Theory and Field Application

Ron Nativ[1,2,3], Jens M. Turowski[3], Liran Goren[1], Jonathan B. Laronne[4], and J. Bruce H. Shyu[5]

[1]Department of Earth and Environmental Sciences, Ben-Gurion University of the Negev, Beer Sheva, Israel, [2]Institute of Earth and Environmental Science, University of Potsdam, Potsdam, Germany, [3]GeoForschungsZentrum, Helmholtz Centre Potsdam, Potsdam, Germany, [4]Department of Geography and Environmental Development, Ben-Gurion University of the Negev, Beer Sheva, Israel, [5]Department of Geosciences, National Taiwan University, Taipei, Taiwan

Abstract Large, rarely mobile boulders are observed globally in mountainous bedrock channels. Recent studies suggest that high concentrations of boulders could be associated with channel morphological adjustment. However, a process-based understanding of large boulder effects on channel morphology is limited, and data are scarce and ambiguous. Here, we develop a theory of steady-state channel width and slope as a function of boulder concentration. Our theory assumes that channel morphology adjusts to maintain two fundamental mass balances: (a) grade, in which the channel transports the same sediment flux downstream despite boulders acting as roughness elements and (b) bedrock erosion, by which the channel erodes at the background tectonic uplift rate. Model predictions are normalized by a reference, boulder-free channel width and slope, accounting for variations due to sediment supply, discharge, and lithology. Models are tested against a new data set from the Liwu River, Taiwan, showing steepening and widening with increasing boulder concentration. Whereas one of the explored mechanisms successfully explains the observed steepening trend, none of the models accuratly account for the observed width variability. We propose that this contrast arises from different adjustment timescales: while sediment bed slope adjusts within a few floods, width adjustment takes a much longer time. Overall, we find that boulders represent a significant perturbation to fluvial landscapes. Channels tend to respond by forming a new morphology that differs from boulder-free channels. The general approach presented here can be further expanded to explore the role of other hydrodynamic effects associated with large, rarely mobile boulders.

Plain Language Summary Large boulders are a significant feature in mountainous landscapes. Recent studies suggested that boulders residing in rivers interfere with the flow and sediment transport, forcing their geometry, specifically width and slope, to change. Our ability to understand and predict such changes is challenged by scarce field data and a general lack of models capable of explaining the processes underlying channel geometry adjustment in the presence of boulders. Here, we develop a theory and several models for the variation of channel width and slope as with channel boulder coverage. Our theory builds on the assumption that the geometry of boulder-bed channels evolves to a new configuration to maintain steadiness of erosion rate and sediment transport. Predictions from the various models are tested against data from the steep Liwu River in Taiwan. These data show that width and slope increase with more boulders. We find that channel slope increases to overcome the greater resistance to sediment transport due to the boulders. In contrast, the scattered nature of the width data and the overall models inability to explain width variability likely reflect a longer adjustment period for width than for slope. This study demonstrates the important role of boulders in shaping landscapes.

Key Points:

- We develop a theory for steady-state reach-scale channel morphology responding to large, rarely mobile boulders in bedrock rivers
- Predictions of boulder-bed channel width and slope are derived based on grade equilibrium and bedrock erosional balance
- Theory is tested against new data from the Liwu River, Taiwan, showing steepening and widening with increasing boulder concentration

Supporting Information:

Supporting Information may be found in the online version of this article.

Correspondence to:

R. Nativ,
ronnat@post.bgu.ac.il

Citation:

Nativ, R., Turowski, J. M., Goren, L., Laronne, J. B., & Shyu, J. B. H. (2022). Influence of rarely mobile boulders on channel width and slope: Theory and field application. *Journal of Geophysical Research: Earth Surface*, *127*, e2021JF006537. https://doi.org/10.1029/2021JF006537

Received 23 NOV 2021
Accepted 29 MAY 2022

Author Contributions:

Conceptualization: Ron Nativ, Jens M. Turowski, Liran Goren
Formal analysis: Ron Nativ
Funding acquisition: Jens M. Turowski
Investigation: Ron Nativ
Methodology: Ron Nativ, Jens M. Turowski, Liran Goren
Project Administration: Ron Nativ
Resources: Jens M. Turowski
Supervision: Jens M. Turowski, Liran Goren, Jonathan B. Laronne, J. Bruce H. Shyu
Validation: Ron Nativ
Writing – original draft: Ron Nativ

1. Introduction

Boulders are ubiquitous in mountainous landscapes, which respond to a large magnitude tectonic perturbations and extreme variability of climatic conditions (Shobe et al., 2021). Boulders with a wide range of diameters, between tens of centimeters and a few tens of meters, can be found on hillslopes (e.g., Bennett et al., 2016; Finnegan et al., 2019; Shobe et al., 2020) and in rivers (e.g., Bathurst, 1996; Pagliara & Chiavaccini, 2006) (Figure 1). Much focus has been given to the effects of small to intermediate sized boulders, with diameters of tens of centimeters to a few meters, on channel hydraulics, channel geometry, and sediment transport (e.g., Carling et al., 2002; Nitsche et al., 2011).

Writing – review & editing: Ron Nativ, Jens M. Turowski, Liran Goren, Jonathan B. Laronne, J. Bruce H. Shyu

A series of recent studies explored the morphological effects of large, rarely mobile boulders, a few meters or more in diameter, which are observed in bedrock rivers (Cook et al., 2018; Shobe et al., 2020, 2021) draining high-relief mountainous terrains. Here, the term "large, rarely mobile boulders", or "large boulders" in short, refers to those grain sizes that are rarely mobile for prolonged durations with expected substantial impacts on long-term geomorphic processes (Haviv, 2007; Huber et al., 2020; Shobe et al., 2021). The emplacement of large boulders is associated with glacial lake outburst floods (Cook et al., 2018), rockfalls, debris flows, landslides, and glacial erratics (e.g., Jouvet et al., 2017; Polvi, 2021). Similar to changes in tectonics and climate, boulder emplacement in rivers can be regarded as a disturbance to the fluvial system, forcing its geometry to adjust in response to the new conditions set by the large boulders. For example, large boulders were argued to affect the scaling relations between channel steepness and catchment-scale erosion rate (Shobe et al., 2018) in comparison to those expected for boulder-free channels (e.g., DiBiase & Whipple, 2011; DiBiase et al., 2010; Lague et al., 2005). Despite these recent insights, the effects of large boulders on channel geometry, especially channel width and slope, have not been systematically studied, and the processes involved in modifications of channel geometry in response to large boulder emplacement have mostly remained unexplored.

Here, we explore the hypothesis that large boulders residing on the river bed can cause channels to alter their width and slope. Our goals are to (a) develop theory that accounts for the effect of large, rarely mobile boulders on channel processes and predicts the expected change in morphologic characteristics with respect to boulder-free channels and (b) compare and contrast the theoretical predictions against new data of channel width, slope, and boulder coverage. The new data of channel morphology and boulder characteristics are based on field and remote sensing observations from the Liwu River in Taiwan, where boulders with diameters of up to 25 m are ubiquitous on the channel bed along river reaches that differ in drainage area and morphology.

2. Background for Large Boulder Control on Channel Geometry

2.1. Effects on Hydraulics and Sediment Transport

Large boulders are macro-roughness elements that enhance flow resistance and alter the flow structure (Nitsche et al., 2011). For example, in mountain streams with relatively shallow flows, boulders exert drag forces on the flow, violating the classic view of a logarithmic velocity profile (e.g., Canovaro et al., 2007; Wiberg & Smith, 1991). Due to the complex three-dimensional flow structure, the spatial distribution of shear stresses considerably varies in the vicinity of boulders, causing local variations in sediment transport (Papanicolaou & Tsakiris, 2017; Papanicolaou et al., 2012). Boulders modify flow patterns around them, such as turbulence intensity, and promote flow accelerations and decelerations (e.g., Tsakiris et al., 2014). In high relative submergence flows, where the water depth is much larger than the boulder diameter, the near-wake zone of a boulder becomes a local region of flow reversals and decelerations (e.g., Dey et al., 2011). It is, thus, expected that such flow regimes favor sediment deposition downstream of boulders (e.g., Papanicolaou & Kramer, 2006).

Boulders and large clasts are thought to reduce the available shear stress for sediment motion (e.g., Buffington & Montgomery, 1997). Coupling theory and flume experiments, Yager et al. (2007) suggested that the drag exerted by immobile boulders could explain why traditional transport equations overpredict bedload fluxes by orders of magnitude. Canovaro et al. (2007) designed flume experiments with different portions of boulder concentrations, demonstrating a humped relationship between the drag stress and boulder concentration. The above studies suggest that bedload flux is reduced in boulder-bed channels due to the strong dependence of bedload transport on the available shear stress (e.g., Nitsche et al., 2011).

2.2. Boulder-Bed Bedrock Channels and Relationships With Channel Slope and Width

Various studies observed links between boulders and channel morphology (e.g., Cook et al., 2018; Lenzi, 2001; Montgomery & Buffington, 1997; Shobe et al., 2018, 2020; Thaler & Covington, 2016; Turowski, Yager, et al., 2009). Recent investigations identified a positive relationship between large boulders and channel steepness index (Thaler & Covington, 2016) and slope (Shobe et al., 2020) in bedrock channels. Steady-state bedrock channel morphology is assumed to reflect long-term adjustment to bedrock river erosion rate in response to the long-term uplift rate (e.g., Whipple & Tucker, 1999). If the uplift rate changes, the river is expected to adjust its profile (e.g., Lague et al., 2005; Whipple, 2004) and cross-sectional geometry (e.g., Turowski, 2020; Turowski, Lague, & Hovius, 2009; Yanites, 2018) such that erosion rates can keep pace with uplift. Assuming immobility

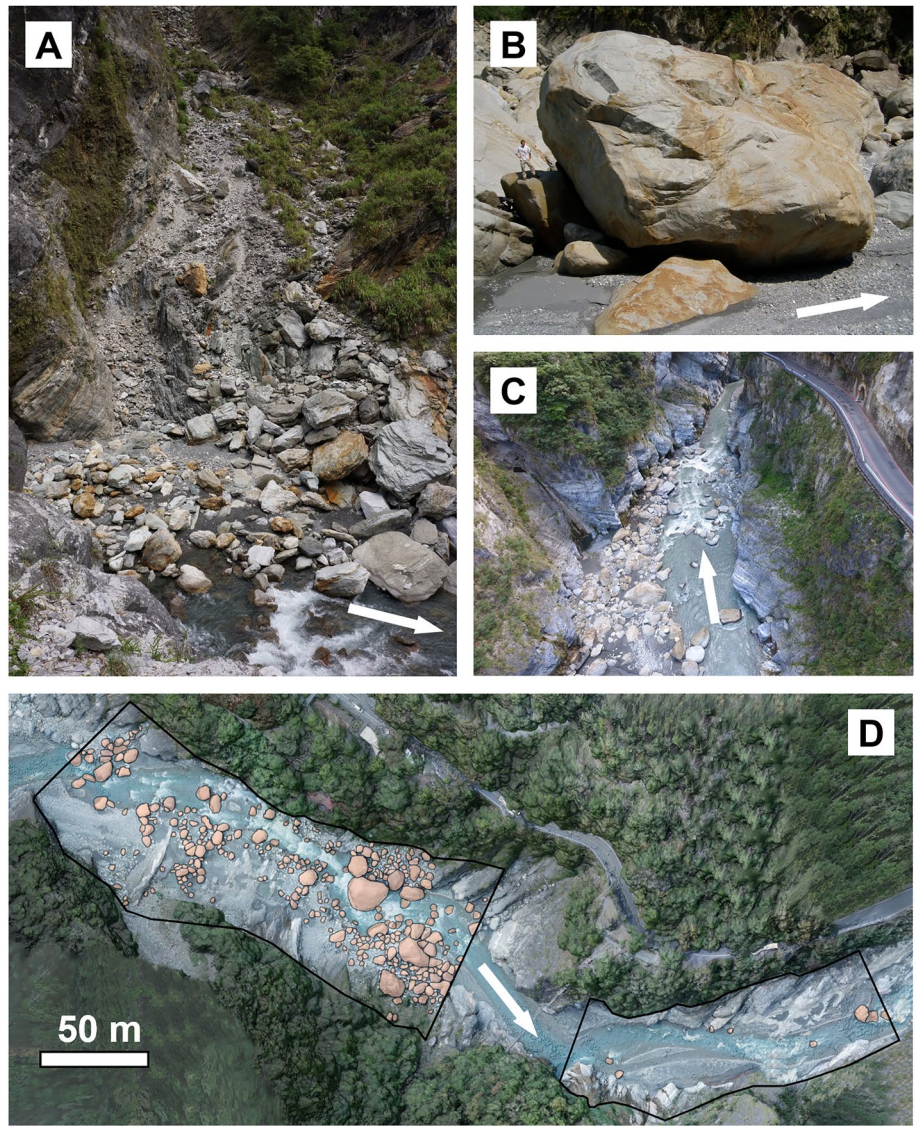

Figure 1. Field photographs from the Liwu River, Taiwan, showing different bed morphologies associated with large boulders. (a) Boulders in a debris channel, indicating an adjacent source of boulders. (b) A large (~15–20 m) boulder downstream of the Marble Gorge. Note the person on the left for scale. (Photograph courtesy: Andrew Wilson). (c) Field evidence for variation in channel width and the relation to boulders in the Taroko National Park, Taiwan. Moving downstream (toward the upper part of the picture), the gorge narrows and boulder concentration decreases. (d) Two neighboring channel reaches with the same drainage area but differing in width and boulder concentration. The black line delineates the channel reach and the orange polygons are boulders with a diameter larger than 2 m. White arrows point to the flow direction.

of large boulders, Shobe et al. (2020) argued that boulders hinder erosion by protecting the bedrock channel bed. Their model predicted that a boulder-bed channel would consequently steepen to compensate for the reduced erosion. Large boulders were also argued to affect bedrock channel width. Shobe et al. (2020) tested the influence of the proximity of the boulder delivery point (e.g., landslides scars) on channel width normalized by drainage area and found that the response is lithology-dependent. Accordingly, conclusive data and a general theory of boulder influence on bedrock channel width are missing.

Bedrock rivers evolve to achieve simultaneous mass balance between bedrock erosion relative to base-level lowering and between sediment transport and supply (Turowski, 2020). The slope of bedrock channels has been argued to adjust both to the requirement of bedrock erosion and upstream supply of sediment (e.g., Sklar & Dietrich, 2006). Still, the degree to which the slope adjusts to each of these components remains unclear

(Johnson et al., 2009). While channel slope is commonly considered to be the consequence of bedrock erosion and reshaping of the longitudinal profile (e.g., Royden & Perron, 2013), recent studies suggested that equilibrium of bedrock channels could be attained by a modification of the slope of sediment overlying the bedrock (Phillips & Jerolmack, 2016; Turowski, 2020, 2021). As in alluvial channels, rearrangement of the bed to form a new sediment-bed slope can be achieved via selective sediment deposition and entrainment during floods (Mackin, 1948; Schneider, Rickenmann, Turowski, & Kirchner, 2015; Schumm & Parker, 1973; Turowski & Hodge, 2017). Furthermore, adjustment of the sediment-bed slope can be achieved within a timescale of a single flood, significantly faster than the timescale associated with bedrock erosion and the formation of a new bedrock slope (Turowski, 2020).

In abrasion-dominated channels, erosion of the bedrock bed and banks is thought to occur during flood events and is driven by impacts of sediment grains, which travel as bedload (e.g., Auel et al., 2017; Cook et al., 2013; Sklar & Dietrich, 2004). Channel widening occurs by lateral erosion, which is thought to be a consequence of sediment particles deflected to the sides following encounters with bed roughness elements (e.g., Li et al., 2020). A field study in a bedrock channel gorge in Switzerland showed that wall erosion increases in proximity to roughness elements (Beer et al., 2017). Although recent studies proposed a positive relationship between lateral erosion and channel roughness (Fuller et al., 2016; He et al., 2021; Li et al., 2020; Turowski, 2018), the precise nature of this relationship and its relation to large boulders remains to be explored (Turowski, 2020).

3. Theoretical Framework

To explore process-based relationships between channel geometry and large boulders, we identify mechanisms by which boulder concentration could affect channel width and slope. Importantly, while sediment bed slope is expected to adjust rapidly in response to external perturbations, including emplacement of large boulders, the timescale of width adjustment is long (Turowski, 2020). This presents an issue, because channel width might not be steady when the perturbations are transient as in the case of boulders. In the current theoretical derivations, we assume that channel width achieves steady-state for a given boulder concentration, which implies that one of the following two conditions prevail: (a) boulder resident time is sufficiently long such that the bedrock channel width has sufficient time to adjust to boulder input; or (b) boulder supply, transport, and degradation balance to keep the concentration of boulders steady over the required timescale of width adjustment. We revisit the validity of these conditions and their potential implications in Section 6.2.

Theory and global observations show that in the absence of other perturbations, channel width increases (e.g., Montgomery & Gran, 2001; Whitbread et al., 2015) and slope decreases (e.g., Wobus et al., 2006) with increasing drainage area. Consequently, to isolate the effects of boulders, the impact of the drainage area needs to be removed. To achieve this, we normalize the steady-state boulder bed width, W_b, and slope, S_b, by the width, W, and slope, S, expected for the same drainage area for a boulder-free channel reach. With this normalization procedure, the theory yields predictions of dimensionless width ratio W_b/W and slope ratio S_b/S.

The geometrical adjustment of a boulder-bed bedrock channel is associated with two aspects of its mass balance. First, bedrock rivers evolve to achieve a steady-state morphology by matching their erosion rate to the uplift rate. Second, similar to alluvial rivers (e.g., Mackin, 1948), the sediment cover of bedrock rivers was argued to evolve toward a graded state (Turowski, 2020), related to the mass balance of river sediments. Aggradation of the bed occurs if the transport capacity is lower than sediment supply, and degradation of the bed occurs when transport capacity is larger than sediment supply. When transport capacity exactly equals sediment supply, the channel is considered graded. Large boulders affect both bedrock erosion and sediment transport. Consequently, the channel geometry is expected to change until an erosion-uplift balance and grade state are met again. As is shown below, the solutions developed under the assumption of erosional balance predict W_b/W as a function of boulder concentration, and predictions derived from the grade assumption yield solutions involving both W_b/W and S_b/S.

3.1. Influence of Boulders on Bedrock Erosion

The erosion rate in abrasion-dominated bedrock rivers is thought to be physically driven by the impacts of moving sediment grains during floods (e.g., Sklar & Dietrich, 1998, 2004; Turowski et al., 2007). When sediment flux increases, more sediment grains are available to impact the channel bed, causing erosion and contributing to the so-called "tools effect" (e.g., Cook et al., 2013). When sediment flux further increases, the bed becomes

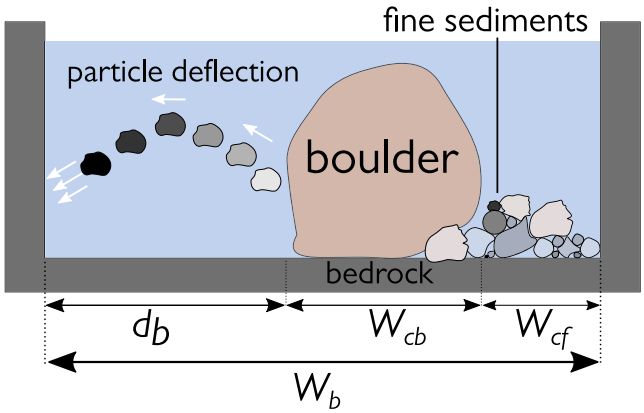

Figure 2. Schematic channel cross-section used in Sections 3.1.1 and 3.1.2. The total boulder-bed channel width W_b is the sum of the different width portions, including boulders (W_{cb}), exposed bedrock, and fine cover (W_{cf}).

shielded from impacts by sediments, consequently inhibiting erosion by the "cover effect" (e.g., Johnson et al., 2010; Turowski & Hodge, 2017). Bedrock erosion is thus modulated by the tools effect, approximated by sediment flux per unit width Q_s/W (kg $s^{-1}m^{-1}$), the cover effect, and the rock erodibility k (m^2kg^{-1}), the latter determining the susceptibility of the rock to erosion. The sediment flux-dependent vertical erosion rate E_v (ms^{-1}) is given by the product of these three terms (Auel et al., 2017; Sklar & Dietrich, 2004; Turowski, 2018)

$$E_v = k\frac{Q_s}{W}(1 - C_f) \tag{1}$$

Here, C_f is defined as the sediment cover due to mobile grains only and does not include the cover by large, rarely mobile boulders. The fine cover can be defined based on a 1D cross-section, as the ratio of the channel width covered by sediments to the total width, W. To predict steady-state channel width using Equation 1, we need an assumption about the steady-state cover. Turowski (2018) suggested that steady-state width can be related to a length scale d (m), which indicates the distance a sediment particle is deflected sideways after impacting a cover patch roughness element, thereby causing bedrock wall erosion. Bedload deflected toward the sidewalls can cause wall erosion if d is larger than the cover-free channel width. In contrast, no wall erosion occurs when d is smaller than the cover-free width. Steady width reflects a condition when the channel width adjusts such that particles almost arrive at the channel wall but do not cause erosion (Turowski, 2018, 2020). Under these conditions, d is equal to the uncovered width

$$C_f = \frac{W - d}{W} = 1 - \frac{d}{W} \tag{2}$$

Substituting Equation 2 with Equation 1 and solving for width, the steady-state width becomes:

$$W = \sqrt{\frac{kdQ_s}{E_v}} \tag{3}$$

The sideward deflection length d is expected to vary in space and time and likely depends on channel hydraulics, roughness, and sediment supply (Beer et al., 2017; Fuller et al., 2016; He et al., 2021; Li et al., 2020; Turowski, 2018, 2020). However, for simplicity, the current analysis assumes that d is constant and uniform.

We explore three potential effects of large boulders on steady-state channel width under an erosional mass balance assumption. For each effect, we develop an analytic expression that predicts a boulder-bed channel width W_{b_m} and then use Equation 3 to normalize it by the steady-state width of a boulder-free equivalent reach. This process leads to terms of the form W_{b_m}/W, where the subscript b stands for a boulder-reach and subscript m denotes the specific effect. When normalizing, we assume that vertical erosion in the boulder-bed channel $E_{v,b}$ equals the erosion rate E_v in an equivalent boulder-free channel reach that transports the same bedload flux and has the same erodibility. Consequently, the erosion rate, bedload flux, and erodibility terms are canceled.

3.1.1. The Cover Effect

Immobile boulders hinder fluvial bedrock erosion by shielding the bed (Shobe et al., 2016, 2018). However, studies that utilized Equation 1 did not consider the presence of rarely mobile boulders with residence times larger than those of fine grains. Here, we consider one end-member response to boulder emplacement in the channel, where boulders encourage fine cover depletion, such that the total cover is not altered. The total cover is the sum of fine sediment cover and boulder cover (e.g., Figure 2). We define boulder concentration Γ to be the ratio of the area covered by boulders to the channel reach area. The riverbed fraction covered by mobile sediments is defined as $C_f = A_f/(A_{tot} - A_b)$, where A_{tot} is the reach area, and A_f and A_b are the areas covered by fine sediments and boulders, respectively. The total cover C_{tot} including mobile sediments and immobile boulders takes a general form of

$$C_{tot} = 1 - (1 - C_f)(1 - \Gamma) \tag{4}$$

Equation 4 can be combined with the equation of erosion rate Equation 1 by replacing $(1 - C_f)$ with $(1 - C_{tot})$, where both C_f and Γ range between zero and one. To illustrate this choice, when Γ is 0.5, half of the channel reach

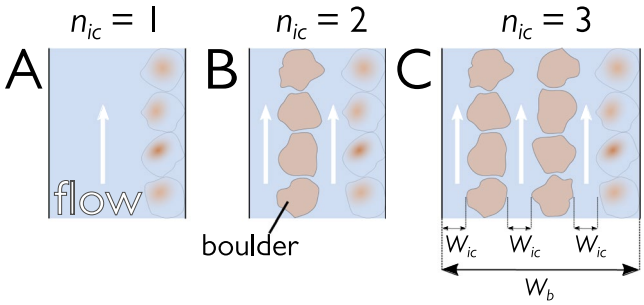

Figure 3. Model geometry used in the multi-channel effect Section 3.1.3. The model delineates a W_b wide fluvial reach hosting columns of boulders. In the cross-sectional direction, one or more in-channels form between two boulder columns or a boulder column and the channel bank. The width of each in-channel is W_{ic}. The total number of in-channels is denoted by n_{ic}. The semi-transparent boulders delineate a scenario in which some boulders are placed adjacently to one of the banks, thus increasing Γ but not changing n_{ic}. For a specific number of in-channels n_{ic}, adding a column of boulders adjacently to the bank does not change n_{ic} but changes Γ (Equation 14). (a) a geometry with $n_{ic} = 1$ and $\Gamma \geq 0$. (b) a geometry with $n_{ic} = 2$. (c) A geometry delineating three in-channels ($n_{ic} = 3$).

area is covered by boulders and half is free to accommodate nonstationary, finer sediments. Then, C_f may be adjusted according to the remaining proportion, for example, $C_f = 1$ means that the fine sediments cover the remaining bed area, a half of the total reach area. However, since the total cover C_{tot} is assumed to be unaltered, it can be described similar to the definition for the fine sediment cover C_f (Figure 2; see also Turowski, 2018)

$$C_{tot} = 1 - \frac{d_b}{W_b} \tag{5}$$

Here, d_b, is the deflection length scale in the boulder-bed channel. Replacing C_f with C_{tot} in Equation (1), substituting Equation (5) into the modified (1), solving for steady-state boulder width W_b, and dividing by Equation 3 leads to:

$$\frac{W_{b_{cover}}}{W} = \sqrt{\frac{d_b}{d}} \tag{6}$$

Equation 6 predicts that the width ratio due to the boulder cover effect, when the total cover is assumed constant, is independent of boulder concentration and only depends on the square root of the ratio of the deflection length scales.

3.1.2. The Tools Effect

In a boulder-bed channel reach, large boulders occupy a fraction of the total bed area, thus reducing the bed area exposed to erosion. We assume that sediments acting as erosion tools can concentrate on such reduced exposed bedrock patches. Consequently, for a given cross-sectional geometry, the existence of large boulders increases bedload flux per unit exposed (or reduced) width, defined here as the effective width W_{eff}. This assumption is somewhat similar to the approach of Yager et al. (2007) and Papanicolaou et al. (2012), who assumed a reduced area for sediment transport. We introduce a parameter α, which controls the magnitude of this effect. The effective width is given by:

$$W_{eff} = W_b(1 - \Gamma)^{\alpha} \tag{7}$$

The condition $\alpha = 1$ implies that sediments only move over the part of the bed without boulders, and $\alpha = 0$ implies that sediments are also transported over the top of the boulders. Within the scope of the tools effect, Equation 1 becomes $E_V = kQ_s/W_{eff}(1-C_f)$, and according to our definition of the fine cover, C_f can be evaluated with $1\text{-}d_b/[W_b(1-\Gamma)]$ (Figure 2). Inserting Equation 7 into the modified Equation 1, solving for steady-state boulder width, and dividing by Equation 3:

$$\frac{W_{b_{tools}}}{W} = \sqrt{\frac{d_b}{d}}(1 - \Gamma)^{\frac{-(\alpha+1)}{2}} \tag{8}$$

According to Equation 8, for $d_b/d = 1$, the tools effect can cause the boulder-bed width to increase with boulder concentration. The combination of the tools and cover effects (TAC) into a single model yields

$$\frac{W_{b_{TAC}}}{W} = \sqrt{\frac{d_b}{d}}(1 - \Gamma)^{\frac{-\alpha}{2}} \tag{9}$$

In this combined model, the width ratio increases with boulder concentration, at a slower rate with respect to the tools model Equation (8).

3.1.3. The Multi-Channel Effect

Immobile boulders are obstacles in the channel, which are hypothesized to form small independent channels ("in-channels") between rows of boulder piles as well as between boulders and the channel banks (Figure 3). The number of in-channels n_{ic} in a boulder-bed reach ≥1. Consider a fluvial reach with a width W_b. There, boulders form island-like columns parallel to the flow direction (Figure 3). Boulder channel width W_b is the sum of the in-channel width W_{ic} times the number of in-channels n_{ic}, and boulder-concentration times channel width

$$W_{b_{MCE}} = W_{ic} n_{ic} + \Gamma W_{b_{MCE}} \tag{10}$$

Here, the acronym MCE stands for a multi-channel effect. The total bedload is assumed to be evenly distributed between the in-channels, such that in each of them, the average bedload flux $\overline{Q_{s\_ic}}$ is given by

$$\overline{Q_{s\_ic}} = \frac{Q_s}{n_{ic}} \tag{11}$$

We assume that steady-state cover independently adjusts within each in-channel so that deflected sediments arrive precisely at the boulder pile or channel bank that bounds the in-channel and do not cause lateral erosion. In this case, a single in-channel width W_{ic} can be approximated using a form of Equation 3

$$W_{ic} = \sqrt{\frac{kd\overline{Q_{s\_ic}}}{E_v}} = \sqrt{\frac{kdQ_s}{E_v}} \frac{1}{\sqrt{n_{ic}}} = \frac{W}{\sqrt{n_{ic}}} \tag{12}$$

Substituting Equation 12 with Equation 10, and solving for $W_{b_{MCE}}/W$, we arrive at

$$\frac{W_{b_{MCE}}}{W} = \frac{\sqrt{n_{ic}}}{1 - \Gamma} \tag{13}$$

Equation 13 predicts channel widening with increasing boulder concentration, where the square root of the number of in-channels sets the magnitude of the effect. The number of in-channels and the boulder concentrations are not independent, as a minimal boulder coverage is needed to bound an in-channel. This restriction can be expressed as a function of boulder grain size D_B:

$$\Gamma \geq \frac{W_{b_{MCE}}}{D_B} (n_{ic} - 1) \tag{14}$$

3.2. Influence on Sediment Transport

According to the concept of grade (Davis, 1902; Gilbert, 1877; Mackin, 1948), a channel removed from equilibrium adjusts its morphology to restore the ability to transport the volume of sediments supplied from upstream. A general mass balance for the sediment-bed elevation, h_s, is described by the Exner equation (Exner, 1925)

$$\frac{\partial h_s}{\partial t} = -\frac{1}{\rho_s (1 - p)} \frac{\partial q_s}{\partial x}, \tag{15}$$

which states that the change of the sediment-bed elevation h_s with respect to time t is proportional to the divergence of sediment mass flux per unit width $q_s = Q_s/W$. Here, the coordinate x denotes the streamwise direction, p is the sediment porosity, and ρ_s is the sediment density. A situation where a channel is in grade entails that the derivative on the left-hand side of Equation 15 equals zero, implying that $\partial q_s/\partial x = 0$ and the sediment flux is constant along the channel.

Based on the above concept, we assume that boulder-bed channels adjust their geometry (i.e., width and slope) with respect to boulder free channels to accommodate the transported sediments in the presence of the boulders. A new equilibrium is reached when the sediment flux within the boulder-bed channel $Q_{s,b}$ matches the sediment flux delivered from an upstream nearby boulder-free channel Q_s. Thus, for equilibrated boulder-bed channels, we can write

$$Q_{s,b} = Q_s \tag{16}$$

To derive the steady-state form of boulder-bed channels, we first define a general bedload transport equation (e.g., Fernandez Luque & Van Beek, 1976; Meyer-Peter & Müller, 1948)

$$\frac{Q_s}{W} = \gamma \left(g \left(\frac{\rho_s}{\rho} - 1 \right) D^3 \right)^{0.5} (\tau^* - \tau_c^*)^{3/2}; \quad \tau^* \geq \tau_c^* \tag{17}$$

Here, $\tau^* = \rho HS/(\rho_s - \rho)D$ is the Shields number, H is flow depth (m), τ_c^* is the critical Shields stress for the onset of bedload motion, D (m) is bedload grain size, g (9.81 ms^{-2}) is the gravitational acceleration, and γ is a

nondimensional constant larger than one (e.g., Wong & Parker, 2006). Assuming a steady flow, using continuity and a flow resistance equation, neglecting the threshold of motion term, and generalizing for width-dependence, Equation 17 can be expressed (e.g., Turowski, 2021) as a water discharge-based equation for sediment transport (Rickenmann, 2001), taking the form of

$$\frac{Q_s}{W^q} = K_{BL} Q^m S^n \tag{18}$$

Here, Q is water discharge ($m^3 s^{-1}$), and K_{BL} is a constant describing transport efficiency. The exponent m typically takes values between 1 and 4 (Barry et al., 2004), while n ranges between 1.5 and 2 (Rickenmann, 2001). The exponent q sets the dependence of bedload transport on channel width and is often assumed to be equal to zero (e.g., Rickenmann, 2001). However, given the unsteady nature of bedload transport and along-stream variations in channel width (Cook et al., 2020), the parameter q may differ from zero. Analytically derived end-member approximations were discussed in Turowski (2021), yielding q values of zero, 0.1, or 2.5.

The influence of boulders on sediment transport can be considered via their potential impact on the various parameters in Equations 17 and 18 (Shobe et al., 2021). First, there might be a reduction in the bedload transport efficiency, K_{BL}, for a given shear-stress (Nitsche et al., 2011; Rickenmann, 2001). Second, a reduction in the effective shear-stress ($\tau^* - \tau_c^*$) could be associated with two different hypothesized effects (Schneider, Rickenmann, Turowski, Bunte, & Kirchner, 2015): (a) a reduction in τ^* due to fluid friction forces (e.g., Canovaro et al., 2007; Nitsche et al., 2011; Yager et al., 2007) and (b) an increase in the threshold of motion τ_c^* (e.g., Lamb et al., 2008; Prancevic & Lamb, 2015). Based on these effects, we establish two theoretical models that predict the relation between width and slope ratios and boulder concentration.

3.2.1. Reduction in the Efficiency of Bedload Transport

A boulder placed into a steady-state channel is expected to change the river's ability to carry bedload sediments. A reduction in transport efficiency is expected because, during a transport event, sediments can (a) be deposited in the wake-zones of boulders due to flow reversals (e.g., Papanicolaou & Tsakiris, 2017; Papanicolaou et al., 2018), thus delaying their overall movement downstream, (b) lose momentum due to direct encounters with boulder-influenced zones (Chiari et al., 2010), and (c) take longer pathways relative to a similar boulder-free channel (e.g., Seizilles et al., 2014). Nitsche et al. (2011) studied flow and bedload transport characteristics in 13 Swiss streams. They showed that fractional transport efficiency K'_{BL}/K_{BL}, where K'_{BL} is the reduced transport efficiency coefficient due to roughness, decreases with boulder concentration. Using digitization of their data (their Figure 8e), we fitted the relation between K'_{BL}/K_{BL} and Γ:

$$\frac{K'_{BL}}{K_{BL}} = \frac{1}{1 + (\theta - 1)\Gamma^{\nu}} \tag{19}$$

Equation 19 is an empirical function with a factor $\theta > 1$ and a power $\nu > 0$. Substituting Equations 18 and 19 with Equation 16 leads to:

$$\frac{S_{b_{STE}}}{S} = \left(\frac{W_{b_{STE}}}{W}\right)^{-q/n} (1 + (\theta - 1)\Gamma^{\nu})^{1/n}, \tag{20}$$

where $W_{b_{STE}}$ and $S_{b_{STE}}$ are the boulder-bed channel width and slope, respectively. The ratios $S_{b_{STE}}/S$ and $W_{b_{STE}}/W$ are both dependent variables, whereas Γ is independent and q, n, θ, and ν are empirical parameters. Closing Equation 20 requires that the width ratio is substituted with either one of the models derived in Section 3.1 or with field data. Assuming a width ratio of one, Equation 20 predicts steepening with increasing boulder concentration.

3.2.2. The Effect of Shear-Stress Partitioning

The total shear stress acting on the river bed is commonly used as a first-order parameter to predict bedload flux (e.g., Equation 17; Einstein, 1950; Fernandez Luque & Van Beek, 1976; Rickenmann, 2001). However, this view is mostly based on flume experiments, where the geometry and roughness are simplified. Natural bedrock channels often exhibit bedforms and large grains, which act as obstacles to the flow, altering water velocity gradients and associated shear stresses. Mainly, roughness elements bear a fraction of the total shear stress τ, thus decreasing the available shear stress for entrainment of bedload τ_{ST}, where the subscript ST denotes sediment transport. Einstein and Banks (1950) suggested that the total resistance to roughness elements equals the sum of

the resistance of each of the individual components. This partitioning approach was later developed for immobile boulders (Yager et al., 2007), and we adopt it here to predict channel width and slope in boulder-bed channels.

Consider a channel with submerged boulders upon which drag forces act (e.g., Bravo et al., 2018). Following Yager et al. (2007), we partition the channel bed into a fine-grained, mobile bedload fraction (denoted by the subscript ST) with a characteristic mobile grain size D and immobile boulders with a diameter of D_B. Shear stresses are not additive, that is, the total shear-stress τ does not equal the sum of all stresses. Instead, forces are additive; hence we can assume a fluid force balance between the driving forces F_{tot} and the resisting forces F_d and F_{ST}

$$\tau A_{tot} = \tau_d A_d + \tau_{ST} A_{ST} \tag{21}$$

Here, $F_{ST} = \tau_{ST} A_{ST}$ is the resisting force due to the roughness of the channel bed without boulders, which encompasses both skin friction and drag (Dey, 2014), $F_d = \tau_d A_d$ is the resisting force due to drag on boulders, and A_{tot}, A_d, and A_{ST} are the channel areas upon which the forces are applied, respectively. The skin friction component due to boulders is assumed to be negligible. Dividing Equation 21 by the total reach area A_{tot}, we obtain

$$\tau = \tau_d \frac{A_d}{A_{tot}} + \tau_{ST} \frac{A_{ST}}{A_{tot}} \tag{22}$$

In a large flood, the entire bed is submerged, and the mobile area, A_{ST}, upon which shear stress applies equals to the overhead projection area without boulders, that is, $A_{ST}/A_{tot} = (1 - \Gamma)$. In contrast, boulders extend into the flow; thus, the drag stresses act mostly on their upstream facing areas. Under the assumption that the overhead projection area is equal to the upstream facing area $A_d/A_{tot} = \Gamma$. Thus, Equation 22 can be rewritten as:

$$\tau = \tau_d \Gamma + \tau_{ST}(1 - \Gamma) \tag{23}$$

We aim to find an expression for the reduced shear stress, τ_{ST}/τ, which we assume is responsible for the transport of all bedload excluding the large boulders. The fractional boulder-drag stress τ_d/τ can be evaluated using a general empirical log-linear model based on experimental results from Canovaro et al. (2007):

$$\frac{\tau_d}{\tau} = \beta\Gamma\left[1 - \ln\left(\frac{\Gamma}{\Gamma_{max}}\right)\right]; \quad 0 < \Gamma \le \min\left(e\Gamma_{max}, 1\right) \tag{24}$$

Here, Γ_{max} is the boulder concentration for which τ_d/τ is maximal, β is a scaling factor, and e is the natural base logarithm. The maximal τ_d/τ value can be derived by applying $\Gamma = \Gamma_{max}$, which leads to $(\tau_d/\tau)_{max} = \beta\Gamma_{max}$. The random-boulder setting experiments of Canovaro et al. (2007) show that Γ_{max} is relatively limited and ranges from ~0.2 to 0.4. The condition $\Gamma \le e\Gamma_{max}$ verifies that τ_d/τ does not yield negative, unrealistic values. Substituting Equation 24 with Equation 23 and solving for τ_{ST}/τ

$$\frac{\tau_{ST}}{\tau} = \frac{1}{1 - \Gamma}\left[1 - \beta\Gamma\left[1 - \ln\left(\frac{\Gamma}{\Gamma_{max}}\right)\right]\right] \tag{25}$$

Considering only the shear-stress partitioning effect, the combination of Equations 16 and 17 implies

$$W_{b_{SSP}} {\tau^*_{ST}}^{3/2} \sim W {\tau^*}^{3/2} \tag{26}$$

when the critical shear stress is neglected. Here, $W_{b_{SSP}}$ is the width of a boulder-bed reach influenced by shear stress partitioning (SSP). Rearranging Equation 26 and solving for $W_{b_{SSP}}/W$ using the definition for the Shields stress $\tau^* = \tau/gD(\rho_s - \rho)$ and $\tau^*_{ST} = \tau_{ST}/gD(\rho_s - \rho)$ and Equation 25

$$\frac{W_{b_{SSP}}}{W} = \left(\frac{\tau_{ST}}{\tau}\right)^{-3/2} = \left[\frac{1}{1 - \Gamma}\left(1 - \beta\Gamma\left(1 - \ln\left(\frac{\Gamma}{\Gamma_{max}}\right)\right)\right)\right]^{-3/2} \tag{27}$$

Equation 27 predicts a non-monotonic relation with boulder concentration. The effect of shear-stress partitioning can alternatively be expressed in terms of the slope ratio (Appendix A)

$$\frac{S_{b_{SSP}}}{S} = \left[\frac{1}{1 - \Gamma}\left(1 - \beta\Gamma\left(1 - \ln\left(\frac{\Gamma}{\Gamma_{max}}\right)\right)\right)\right]^{\frac{\delta - 0.5}{\delta + 0.5}} \tag{28}$$

where δ is an exponent relating water velocity to the hydraulic radius R_h and equals ½ for a Darcy-Weisbach relation or ⅔ for a Manning-Strickler relation. For δ equals ½, the right-hand side of Equation 28 equals one, and the boulder-bed channel slope S_b equals the boulder-free channel slope, whereas when δ equals ⅔, the slope ratio S_b/S depends on the expression on the right-hand side of Equation 28 to the power of 1/7. With such a low exponent, the effect of shear-stress partitioning on the slope ratio is expected to be small.

4. The Liwu River: Methods and Field Application

The Liwu River, Taiwan, exhibits multiple fluvial bedrock reaches hosting large boulders with diameters that range from 2 to over 20 m. We utilize this unique setting to explore the effects of large, rarely mobile boulders on channel width and slope in a natural setting, and to compare the emergent relations to the theory and mechanisms developed in the previous section.

4.1. The Liwu River, Taiwan

Taiwan is an active orogen that emerged from a collision between the Luzon Arc and the Asian passive margins. The ongoing collision is thought to have initiated in the late Middle Miocene (~12 Ma) (Teng, 1990). Due to its location in the Pacific, Taiwan is frequently hit by typhoon storms (an average of four per year; Dadson et al., 2003). The Liwu River drains 630 km^2 of steep mountainous terrain on the eastern flanks of the Taiwanese massif (Figure S1 in Supporting Information S1). It originates from 3,500 m a.s.l and drains in the Pacific Ocean through varying lithological facies. Basin geology comprises metamorphic rocks with variable grades ranging from gneiss and marbles in the lower part, mostly schist in the middle part, and phyllites, slates, and metasandstones in the upper part of the basin (Figure S1 in Supporting Information S1). Typhoon floods generate high water discharges in the river a few orders of magnitude larger than daily average discharges (Hartshorn et al., 2002; Lague et al., 2005). Extreme precipitation events and floods are also expected to cause elevated sediment supply rates (Cook et al., 2013; Hovius et al., 2000; Turowski et al., 2008).

4.2. Methods

We documented 20 fluvial reaches along the Liwu River. Field data were collected during the low flow seasons of 2018 and 2019. We selected different fluvial reaches with variable local relief, representing various portions of the drainage basin. Some of the reaches were tributaries with drainage areas, A that range between 60 and 200 km^2, while other reaches belong to the main Liwu river trunk (A = 250–520 km^2). Our primary focus was directed to channel segments with a substantial number of boulders, but we also collected data from channels with a lower boulder concentration. The reach length was chosen to represent approximately uniform boulder-covered bed areas, with two to six times the reach width. Documented reaches are characterized by a uniform local lithology and no side tributaries. In each channel reach, a drone was flown at 80–120 m above the channel to document the topography, constrained by the complexity of the topography and the pilot's location.

Point clouds were generated using the Agisoft Metashape commercial software, utilizing a Structure from Motion algorithm (Westoby et al., 2012). The point clouds were used for generating orthophotos and DEMs at 5–25 cm/pixel, depending on data quality. Due to the steep topography of many bedrock canyon sections, most of the reaches were inaccessible by foot, thus prohibiting the emplacement of ground control points (GCPs). To evaluate a representative error on elevations extracted from our drone-derived DEMs, we performed a representative drone survey in the Baiyang site having nine GCPs and using a Differential GPS to document their locations (Table S1 in Supporting Information S1). Then, we generated a DEM for the site while excluding the GCPs as inputs. The vertical standard error of elevation error could be calculated using this method by comparing the non-registered DEM and the GCP coordinates. The standard error of elevation was 45 cm, and in the following, we use a conservative elevation error of 0.5 m for slope calculations (Text S2 and Figure S2 in Supporting Information S1). Based on the similarity of drone survey parameters among the various studied reaches, we apply the same vertical elevation error for the slope calculations for all our studied reaches.

The reach area A_{tot} was manually delineated using a digitization process in ArcGIS. First, the upstream and downstream channel reach boundaries were chosen and delineated with straight lines, bounding what we observed as an approximately continuous distribution of boulders (Figure 4). Second, the boundaries of channel banks were

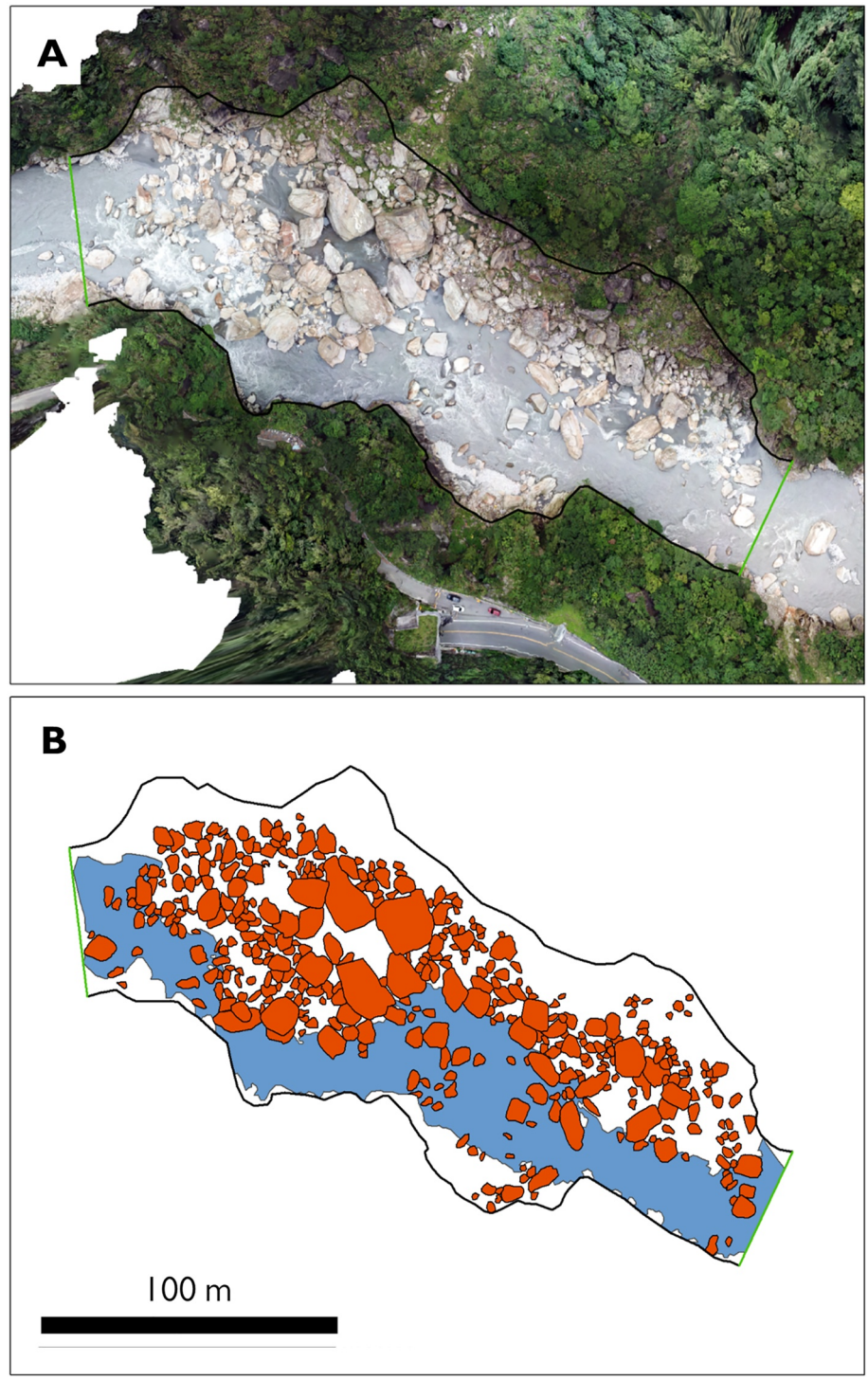

Figure 4. An example of boulder digitization. (a) A 3D model-derived orthophoto. The channel reach boundaries are marked (outer black and green lines). (b) The observed boulders are manually digitized (orange polygons). Boulder concentration was calculated using the sum of all boulder area divided by the reach area. For this calculation, we accounted only for boulders with a diameter >2 m. Flow direction is from left to right. Green lines in the upstream and downstream reach margins are the locations where cross-sections were used to estimate the reach-scale channel slope. For illustration, the water flow is shown in blue.

identified and tracked by following distinctive bedrock-vegetation contacts. To evaluate the boulder concentration in the channel reach, we manually digitized the map-view area of all the visible boulders with a diameter ≥2 m (Figure 4b). A boulder was commonly recognized by observing that it protrudes from water or a gravel bar. An estimate of boulder concentration was calculated for each reach using the relation $\Gamma = A_b/A_{tot}$, where $A_b = \Sigma A_B$ is the sum of the areas of all of the boulders. Reach-averaged channel width W_b was calculated by dividing the reach area by the thalweg length L, the assumed streamwise distance that follows the curvature of the map-view channel banks. The thalweg length L was digitized by hand on an orthophoto, considering a 5 m uncertainty on its measurement. An alternative method for calculations of W_b was applied for comparison; it is shown in the Figure S3 in Supporting Information S1. To calculate reach-scale channel slope S_b in a boulder-bed channel, the cross-sections that define the upstream and downstream boundaries of the reach area (Figure 4) were extracted from the DEM. The minimum elevation of the downstream cross-section was subtracted from the minimum elevation of the upstream cross section and divided by L. Because a substantial fraction of the bedrock bed is occupied with fine sediments, this slope represents a sediment-bed slope, which might differ from the bedrock-bed slope.

For each measurement of S_b and W_b in a boulder-bed reach, we define S and W to be the slope and width of a boulder-free channel with an equal drainage area. Calculations of W and S were performed utilizing a basin-wide scaling relationship against the drainage area for channel segments with no or few boulders (Figure S4 in Supporting Information S1).

5. Results

5.1. Channel Morphology and Boulder Concentration

The data we collected include channel reaches with widths ranging between 30 and 120 m, slopes ranging from 0.01 to over 0.08, and boulder concentrations that range between ∼0 and 0.34 (Table 1 and Figure 5). We observe that both the channel width (Fig. 5a; $R^2 = 0.29$) and slope (Fig. 5b; $R^2 = 0.51$) tend to increase with boulder concentration Γ. The increasing trend with boulder concentration is more distinct when considering the width ratio W_b/W (Figure 5c; $R^2 = 0.42$) and slope ratio S_b/S ($R^2 = 0.71$). In both cases, normalization by W and S improves the relationship with Γ, as indicated by the increase in R^2 using a least-square power-law regression (Figure 5). p-values evaluated using T-tests for the various relationships in Figure 5 demonstrate that they are statistically significant. Although the width ratio exhibits scatter for a given Γ, W_b/W is always larger than unity for $\Gamma > 0.05$. The width ratio exhibits two sub-trends distinguished by the two data points with largest W_b/W values where $\Gamma \sim 0.15$. The slope ratio increases from slightly below one for $\Gamma \sim 0$ to almost four for $\Gamma \sim 0.35$. The slope ratio is always larger than one when boulder concentrations are larger than 0.1. Fifteen among the 20 reaches lie within a schist lithology, while the other reaches are incised into gneiss. Lithological differences cannot explain the scatter in the width and slope ratios (Figure S6 in Supporting Information S1).

5.2. Model Evaluation Using the Liwu River Data

The mechanisms developed in Section 3 to explain variations in width and slope in boulder-bed channels (see summary of models in Table 2) are tested against the Liwu River data (Table 1). Each model contains various parameters, some of which could not be independently constrained. We emphasize that the Liwu River width ratio show significant scatter for a given boulder concentration, and none of the field parameters we explored could collapse the width ratio data and reduce its overall scatter. Therefore, we cannot expect a single combination of parameters to explain the width ratio data as a whole.

5.3. The Tools, Cover, "Tools and Cover," and Multi-Channel Effect Models

To examine the performance of the models against the data, we compare them against a trivial case in which the widths of boulder-bed and boulder-free channels are similar. Such a situation, with $W_b = W$ yields RMSE value of 0.48. The cover (Equation 6), the tools (Equation 8), and the combined 'tools and cover' (Equation 9) effects are directly compared to the field data. For simplicity and because the relationship between boulder-related deflection length d_b and boulder concentration is unknown, we assume $d_b/d = 1$ throughout the analysis. We first note that the cover model is independent of boulder concentration (Figure 6). Its prediction does not follow the trend observed in the field data and is equivalent to a case where $W_b = W$, yielding a RMSE value of 0.48 (Table 2).

Table 1
Liwu River Data

	[a]Channel reach name	Drainage area, A (km^2)	Boulder-bed channel width W_b (m)	[b]Boulder-free channel width W (m)	Boulder-bed channel slope S_b	[c]Boulder-free channel slope S	Boulder concentration, Γ	Mean boulder size D_{mean} (m)	Maximal boulder size D_{max} (m)
1	Baiyang downstream	59	40.6	33.6	0.021	0.055	0.05	2.9	6.2
2	Baiyang upstream	59	29.9	33.6	0.039	0.055	0.10	4.0	7.5
3	Bouluwan downstream	507	59.7	55.9	0.023	0.018	0.04	3.3	12.2
4	Bouluwan upstream	507	76.4	55.9	0.054	0.018	0.34	4.4	19.5
5	Dasha park	186	45.5	44.0	0.052	0.031	0.17	4.0	15.4
6	Dasha red-bridge downstream	183	60.3	43.9	0.034	0.031	0.07	2.0	9.1
7	Dasha red-bridge upstream	183	53.8	43.9	0.045	0.031	0.09	2.6	7.9
8	Dasha tunnel downstream	179	68.3	43.6	0.084	0.031	0.29	4.1	15.2
9	Dasha tunnel upstream	179	43.2	43.6	0.026	0.031	0.03	3.4	5.5
10	East baiyang (near the parking)	188	39.3	44.2	0.033	0.030	0.05	1.7	10.4
11	Heliu camp Downstream	431	46.8	53.8	0.026	0.020	0.02	3.4	7.1
12	Heliu camp upstream	431	71.7	53.8	0.038	0.020	0.24	2.6	17.2
13	Lushui	450	83.7	54.3	0.022	0.020	0.22	4.4	23.4
14	Lushui Downstream	431	104.5	53.8	0.040	0.020	0.15	3.3	12.4
15	Lushui Upstream	431	56.5	53.8	0.012	0.020	0.01	2.2	3.6
16	Ning an Upstream	523	124.4	56.3	0.024	0.018	0.16	3.5	23.2
17	Sinuous reach	523	102.9	56.3	0.064	0.018	0.29	3.0	19.1
18	Sinuous upstream	514	84.4	56.1	0.018	0.018	0.10	2.1	12.2
19	Tianxiang construction	431	67.6	53.8	0.047	0.020	0.20	3.3	17.3
20	Tianxiang hotel	258	54.0	47.6	0.048	0.026	0.16	2.5	19.2

[a]Boulder-bed reach locations are shown in Figure S1 in Supporting Information S1. [b]Boulder-free width was calculated using a basin-scale relationship with drainage area $W = 0.48\,A^{0.24}$ for channels without boulders (Figure S4 in Supporting Information S1). [c]Boulder-free channel slope was calculated using the relation $S = 505.4\,A^{-0.51}$ for channels without boulders (Figure S4 in Supporting Information S1).

The tools and the "tools and cover" effects contain one free parameter, α, which could vary between zero and one. In the case of $\alpha = 0$, the tools model predicts widening with respect to boulder concentration and yields a RMSE value of 0.40, while the tools and cover model predicts the trivial case of $W_b = W$. For $\alpha = 1$, the tools effect predicts a greater widening with boulder concentration (Figure 6), with a model-data RMSE of 0.33 (Table 2). Although the RMSE value is lower than that of the trivial model, the tools effect underpredicts most of the data. For $\alpha = 1$, the tools and cover model predicts widening with increasing Γ, yielding a RMSE value of 0.40.

The multi-channel effect, Equations 13 and 14, is tested with the number of in-channels, n_{ic} in the range of one to four. The model generally mimics the increase in W_b/W seen in the field data (Figure 7). Models using $n_{ic} = 1$, 2, and 3, capture 80%, 25%, and 10% of the data, respectively. Altogether 19 data points (95%) can be explained by the model using an n_{ic} of 1 or 2. The RMSE decreases for smaller n_{ic} values (Table 2) with a minimal value of 0.33 for $n_{ic} = 1$.

5.4. Reduction in Sediment Transport Efficiency

The model of the reduction of sediment transport efficiency, Equation 20, combines both the width and slope ratios and therefore requires a second equation or independent data to close the system. Furthermore, to solve Equation 20, the parameters q, n, θ, and ν need to be constrained. The parameter q was shown to take specific values of 0, 0.1, 1, and 5/2 (Section 3.2.1). We study the behavior of the model for a variable q, since it determines the magnitude in the covariance of channel width and slope. We first note that the Liwu data show a somewhat positive correlation of the slope ratio with increasing width ratio (Figure S7 in Supporting Information S1) with much scatter for a given W_b/W. For each q value explored, we iterated random values of the remaining unknown

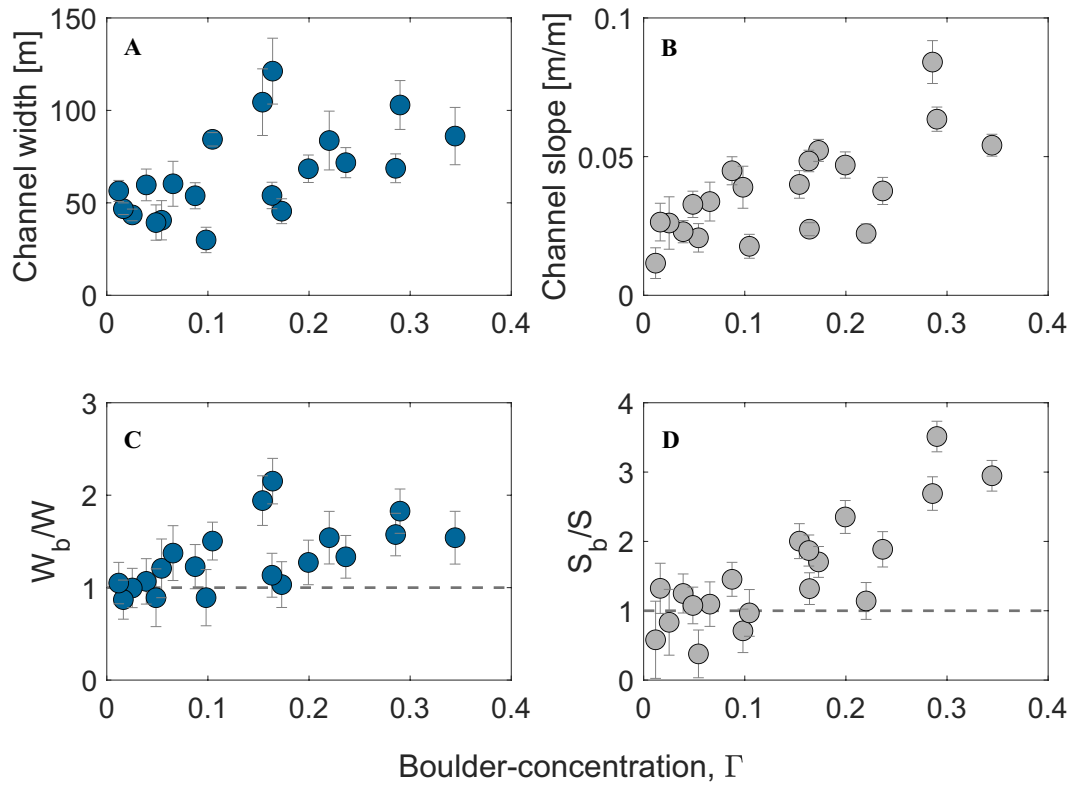

Figure 5. Channel morphology versus boulder concentration in the Liwu River. (a) Channel width increases with boulder concentration ($R^2 = 0.29$). Error bars represent one STD from the mean of ten along-reach measurements. (b) Channel slope increases with boulder concentration ($R^2 = 0.51$). Error bars represent uncertainties in edge elevation (0.5 m) and in thalweg length (5 m). (c) The width ratio W_b/W increases with Γ ($R^2 = 0.42$). (d) The slope ratio S_b/S increases with Γ ($R^2 = 0.71$). For information about the errors associated with calculations of W_b/W and S_b/S, see supporting information.

parameters: n, θ, and ν from a range of values (see caption of Figure 8 for more details), selecting those that minimized the RMSE value between the model output and the Liwu data. Utilizing the width ratio of the Liwu River (Table 1) to close the system, when q is low (i.e., equals zero or 0.1), the model captures the increase in S_b/S with Γ (Figure 8). In contrast, for larger values of q, the model deviates significantly from the data. The model performs best with a lowest RMSE value of 0.43 (relative to a trivial case, in which $S_b = S$ and RMSE = 0.98) when q is close to or set to zero (Table 2), which corresponds to a case where the slope ratio S_b/S is independent of the width ratio W_b/W.

5.5. The Effect of Shear-Stress Partitioning

We test the shear-stress partitioning model against the Liwu River width and slope ratios independently. To test the model, we varied either β or Γ_{max}, while treating the other as a constant (see below). The parameter β defines how fast the normalized drag stress increases with increasing Γ (Equation 24), and Γ_{max} is the boulder concentration corresponding to the maximal normalized drag stress. Both parameters were only constrained from flume experiments (Canovaro et al., 2007). Based on the digitization of Canovaro et al. (2007) data, β ranges between 1.8 and 4.2, while Γ_{max} varies from 0.18 to 0.37. Here we explore a wider range that better fits the field data. We tested Equation 27 by first plotting model predictions using a constant $\Gamma_{max} = 0.6$ and exploring a range of β values. Then, $\beta = 1$ was held constant and Γ_{max} was varied to study its control on model behavior.

We find that the model predicts a non-monotonic trend between boulder concentration and the width ratio. At small boulder concentrations, the width ratio increases, then it reaches a maximum, after which it decreases with increasing boulder concentration (Figure 9). With increasing β, the width ratio maximal value shifts toward larger Γ and larger W_b/W values (Figure 9a). A similar behavior is observed when increasing Γ_{max} (Figure 9b). We test the likelihood that the data can be described by a non-monotonic model by evaluating a Spearman's rank

Table 2
Models Performances of the Width and Slope Ratios

Assumption	Mechanism	Equation	Prediction	[a]Parameters	[b]RMSE	Figures
Erosional balance: bedrock erosion matches between boulder-bed and boulder-free channels	Cover	$W_{b_{cover}}/W = \sqrt{d_b/d}$	Independent of Γ	$d_b = d$	0.48	2, 6
	Tools	$W_{b_{tools}}/W = \sqrt{d_b/d}(1-\Gamma)^{-(\alpha+1)/2}$	Widening	$\alpha = 0$	0.40	2, 6
				$d_b = d$		
			Widening	$\alpha = 1$	0.33	
				$d_b = d$		
	Tools and cover	$W_{b_{TAC}}/W = \sqrt{d_b/d}(1-\Gamma)^{-\alpha/2}$	Independent of Γ	$\alpha = 0$	0.48	2, 6
				$d_b = d$		
			Widening	$\alpha = 1$	0.40	
				$d_b = d$		
	Multi-channel effect	$W_{b_{MCE}}/W = \sqrt{n_{ic}}/(1-\Gamma)$	Widening	$n_{ic} = 1$	0.33	3, 7
				$n_{ic} = 2$	0.45	
				$n_{ic} = 3$	0.78	
Grade: equal sediment flux between boulder-bed and boulder-free channels	Reduction in sediment transport efficiency	$\frac{S_{b_{STE}}}{S} = \left(\frac{W_b}{W}\right)^{-q/n}(1+(\theta-1)\Gamma^{\nu})^{1/n}$	Steepening	$q = 0$	0.43	8
				$q = 0.1$	0.44	
				$q = 1$	0.76	
	Shear-stress partitioning	$\frac{W_{b_{SSP}}}{W} = \left[\frac{1}{1-\Gamma}\left(1-\beta\Gamma\left(1-\ln\left(\frac{\Gamma}{\Gamma_{max}}\right)\right)\right)\right]^{-3/2}$	Non-monotonic	$\beta = 0.97$	0.29	9
				$\Gamma_{max} = 0.57$		
				$\delta = 0.67$		
		$\frac{S_{b_{SSP}}}{S} = \left(\frac{1}{1-\Gamma}\left[1-\beta\Gamma\left[1-\ln\left(\frac{\Gamma}{\Gamma_{max}}\right)\right]\right]\right)^{\frac{\delta-0.5}{\delta+0.5}}$	Non-monotonic	$\beta = 1.38$	0.50	10
				$\Gamma_{max} = 0.30$		

[a]The parameter values used to examine the models against the Liwu data (Section 5). [b]Root Mean Square Error (RMSE) calculated between the Liwu data and the examined model.

correlation coefficient between the width ratio and boulder concentration. A calculated value of 0.65 implies that the two variables are positively correlated. However, a non-monotonic relationship cannot be ruled out.

Considering the effect of the shear-stress partitioning on the slope ratio, in Section 3.2.2, we showed that the slope ratio depends on boulder concentration to a maximum power of 1/7. Regardless of the choice of the other free parameters, this produces only a weak dependence between the slope ratio and boulder concentration, which makes the shear-stress partitioning model inadequate to describe the Liwu River slope ratio data (Figure 10).

6. Discussion

6.1. Evaluation of the Theoretical Models

Under the two steady-state assumptions described in Section 3, we have proposed five mechanisms presumably underlying the adjustment of channel morphology to the presence of large, rarely mobile boulders (Table 2).

Five models have been considered for the width ratio, W_b/W: the cover, the tools, the "tools and cover," a multi-channel effect, and a shear-stress partitioning effect. The cover effect is shown to be independent of boulder concentration. This result is an outcome of the assumption that the total cover is unchanged when boulders are placed into the channel. Instead, the total cover adjusts such that fine cover is removed and the exposed bedrock area ultimately remains constant. In this model, the principle disturbance that the channel experiences as a result of boulder emplacement is a reduced erosion. The channel could respond by altering its state variables: width, slope, and fine cover, such that erosion can be increased to match tectonic uplift again. Hence, the end-member

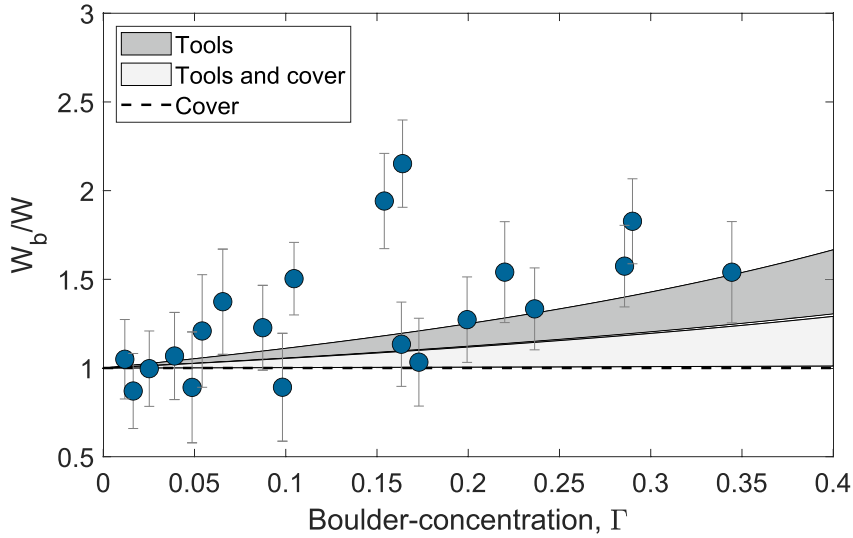

Figure 6. The width ratio W_b/W versus boulder concentration (Γ) compared between the Liwu River field data (blue circles) and three models: (I) the tools effect (Equation 8; dark gray shaded area depicts the model output range when the parameter α is varied between zero and one), (II) the "tools and cover" effect (Equation 9; light gray shaded area, using the same α range as in the tools effect), and (III) the cover effect (Equation 6; black dashed line) predicts the width ratio to be independent with respect to boulder concentration. All models are plotted assuming $d_b/d = 1$.

described by Equation (6) is plausible if as a result of a reduced erosion, the channel steepens, transport capacity increases, and fine cover reduces. A second end-member response can be described by a cross-section that widens to maintain the same uncovered area. Such an approach is not taken in this study, but should be considered in future studies.

According to the tools effect, in the presence of boulders, the tools impact an effectively smaller bedrock area, which increases bedrock erosion. The channel then adjusts by increasing its width to decrease the reach-averaged erosion rate to the background uplift rates. Importantly, independent consideration of the tools effect and the

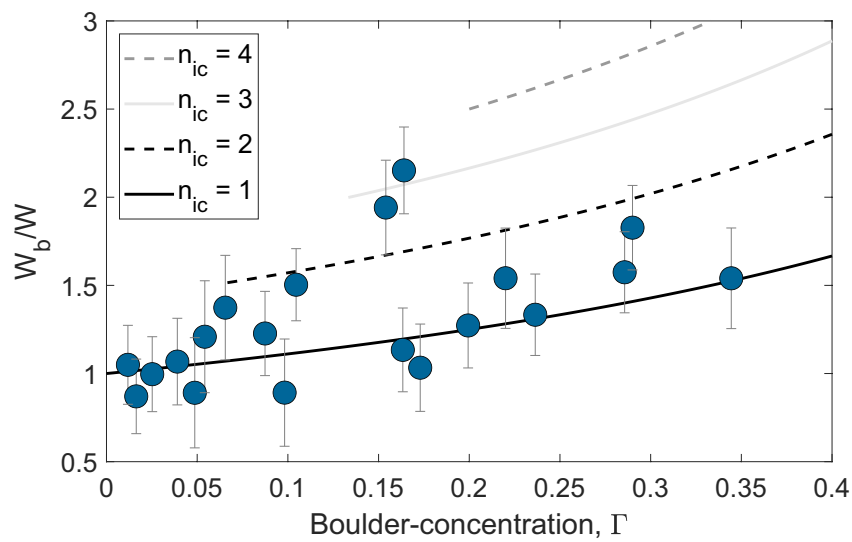

Figure 7. The width ratio W_b/W versus boulder concentration Γ compared between the Liwu River field data and the multi-channel effect model (Equation 13). The width ratio data are plotted versus boulder concentration (blue circles). Curves represent the multi-channel model with a different number of in-channels n_{ic} (see legend). Note that the model curves are constrained by a threshold value of Γ, calculated with Equation 14 by using a minimal boulder size $D_B = 2$ m and boulder-bed channel width $W_b = 30$ m.

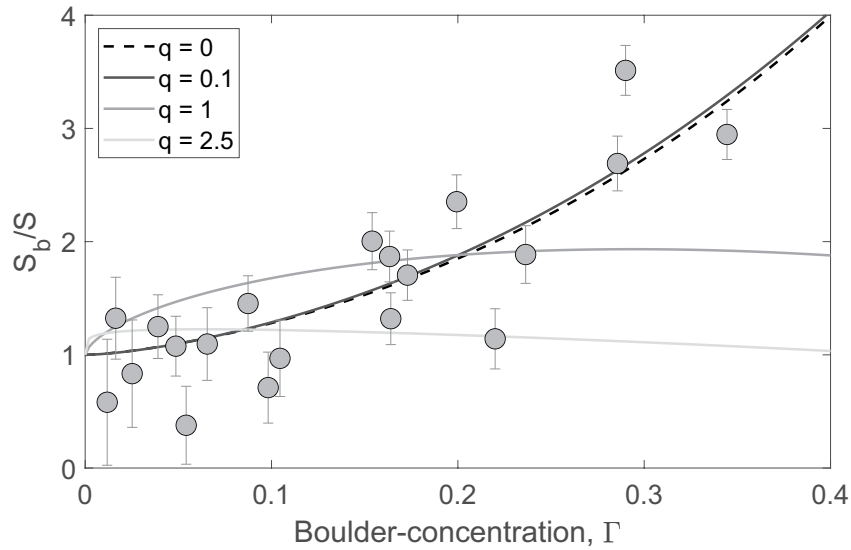

Figure 8. The slope ratio S_b/S versus boulder concentration Γ compared between the Liwu river field data (gray circles) and the reduction in transport efficiency model (Equation 20). For each selected q value (see legend), we varied $0 \le n \le 5$, $0 \le \theta \le 25$, and $0 \le \nu \le 5$, and documented the resultant RMSE value between the model and Liwu slope ratio S_b/S. The plotted curves are model predictions for which the RMSE values were the lowest. Note the deviation of the model from the data for larger q values (i.e., for q values of 1 and 2.5). See Table S2 in Supporting Information S1 for the best-fit parameter values used in this plot.

cover effect may be limiting when comparing against data. In our treatment of the cover effect, bedload particles move over the boulders because the effective width (W in Equation 1) is not assumed to change. However, in this case, the bedload transport rate effective for erosion changes because a fraction of the bedload ceases to contribute to bed erosion.

The combined "tools and cover" effect, Equation 9, predicts a small spectrum of channel adjustment, ranging from boulder independence ($\alpha = 0$) to a slight widening ($\alpha = 1$)—see Figure 6. The essential difference between

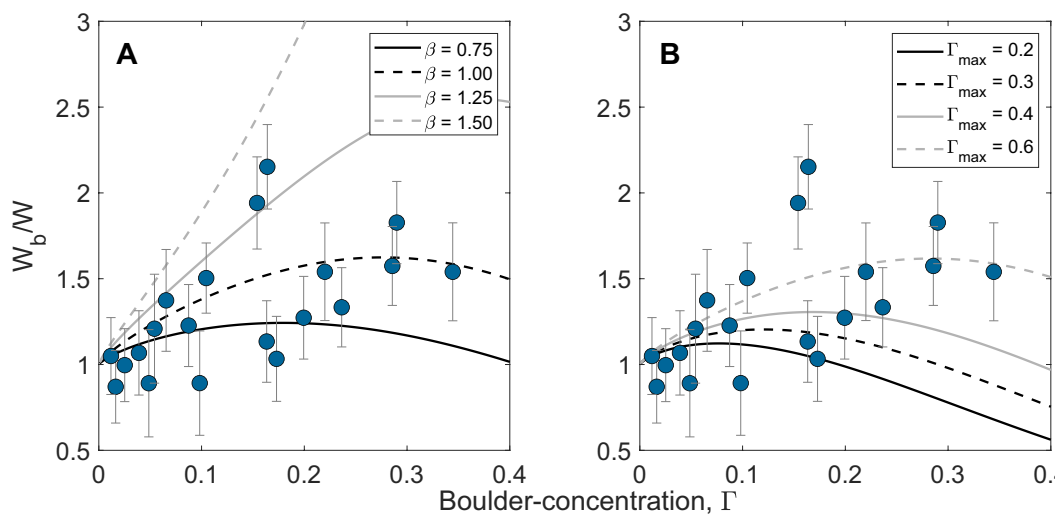

Figure 9. The width ratio W_b/W versus boulder concentration Γ compared between the Liwu river field data (blue circles) and the shear-stress partitioning model using different model parameters. (a) The parameter $\Gamma_{max} = 0.6$ is kept constant while β is varied between 0.75 and 1.50. Model scenarios (black and gray curves) show that the width ratio increases with boulder concentration, but then reaches a maximum, after which it decreases. The maximum width ratio for each scenario increases with increasing β. (b) The parameter $\beta = 1.00$ is kept constant whereas Γ_{max} is varied between 0.2 and 0.6. As in (a), this figure indicates a humped relationship, with a maximum width ratio that increases with Γ_{max}.

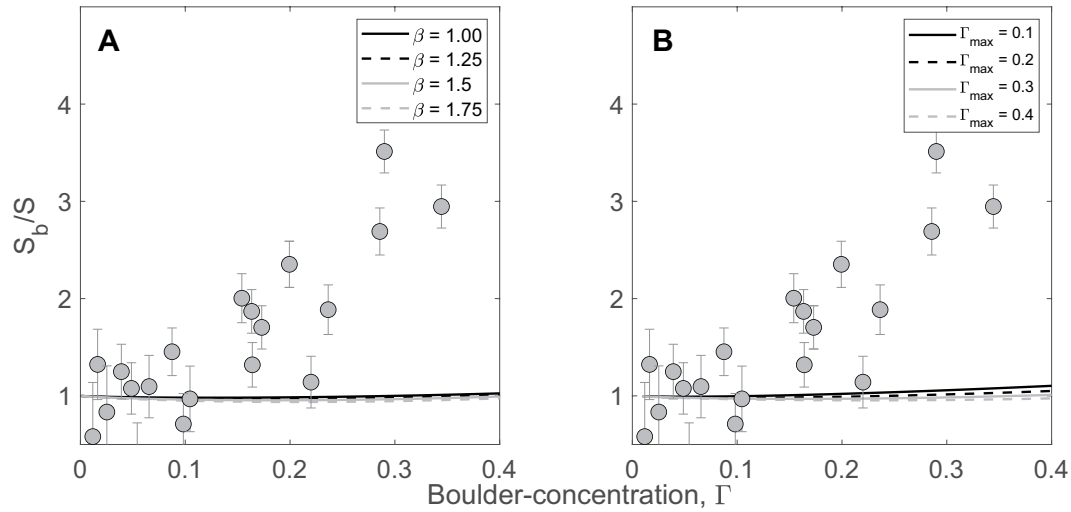

Figure 10. The slope ratio S_b/S versus boulder concentration Γ compared between the Liwu river field data (gray circles) and the shear-stress partitioning model (Equation 28) using different model parameters, and $\delta = ⅔$ a constant. (a) The parameter $\Gamma_{max} = 0.30$ is kept constant while β is varied between 1.00 and 1.75. The model scenarios (black and gray curves) show that the slope ratio first decreases and then slightly increases with boulder concentration but do not capture the Liwu River slope ratio. (b) The parameter $\beta = 1.25$ is kept constant whereas Γ_{max} is varied between 0.1 and 0.4.

the tools and tools and cover models is the exponent of $(1-\Gamma)$, which depends on the parameter α, describing whether bedload particles are routed above boulders ($\alpha = 0$) or in between boulders ($\alpha = 1$). At the process scale, large boulders protruding into the flow are thought to encourage sediment deposition around them (e.g., Papanicolaou & Kramer, 2006; Polvi, 2021; Tsakiris et al., 2014), which may lead to substantially different protrusion, causing bedload transport to alter significantly (Yager et al., 2007). We, therefore, expect that boulder protrusion and hydraulic behavior near boulders play an essential role in controlling α.

The tools, cover, and "tools and cover" models additionally scale linearly with the square root of boulder-bed to boulder-free deflection lengths, which we assumed to be one, that is, $d_b = d$. However, previous research implies that the deflection length ratio could differ from one (Beer et al., 2017; Fuller et al., 2016; He et al., 2021; Li et al., 2020). The influence of boulder concentration on sediment deflection is unknown, but a positive correlation may account for channel widening for the above-discussed models beyond the predictions with $d_b = d$.

The multi-channel effect (Equation 13) predicts an increase in the width ratio with boulder concentration with a magnitude that depends on the square root of the number of in-channels (Figure 7). Using this one free parameter, the model captures a substantial fraction of width variability among the examined reaches in the Liwu River, despite its overall scatter. Notably, the geometry associated with $n_{ic} = 1$ (e.g., Figure 3), which produces the minimal RMSE, is one where the boulders coat the wall, which is not entirely consistent with field observations (Figures 1d and 4).

We propose three major potential causes for the deviations between the multi-channel model and data relating to the three model assumptions: (a) the channel reach follows a specific geometry, including boulder arrangement (Figure 3). The Liwu boulder-bed channel reaches, however, exhibit a wide range of boulder sizes and inner-reach distributions. (b) Sediments are redistributed evenly between the in-channels. Nonetheless, at bankfull flows, when the entire bed is submerged, sediments are expected to follow paths set by the flow hydrodynamics—rather than the configuration of boulders—and not necessarily to be evenly distributed. (c) The overall boulder-bed channel width reflects a steady-state configuration for every in-channel independently. We discuss the assumption of a steady-state configuration in terms of channel width in Section 6.2. Ultimately, to better describe a multi-channel effect, specific treatments of boulder distributions and sediment paths should be considered.

The effect of shear-stress partitioning shows a humped relationship between the width ratio and Γ. Although the model captures 65% of the data within error, we emphasize two reasons for the model's inadequacy to explain the Liwu data. First, a simpler, linear model could also account for the same data fraction captured by the non-monotonic model. Second, to better predict the data, the parameters β and Γ_{max} likely need to differ between

the different reaches, but independent constraints on their values are missing. Since the physical interpretation of β is unclear, we cannot evaluate the extent to which this parameter should vary among the examined reaches.

The general scatter in the width ratio (Figure 5) and overall inability of our proposed models to account for width variability lead us to suspect that different reaches in the Liwu River have adjusted to boulder input to various degrees. Such variability probably reflects long adjustment timescales for the channel width. Indeed, theoretical considerations show that the adjustment timescale for bedrock reaches responding to perturbations is in the order of 10^3–10^5 years (Turowski, 2020).

Two models have been considered for the slope ratio, S_b/S: reduction in transport efficiency and shear-stress partitioning. Both were developed under the assumption of grade. Due to its very small exponent value, the effect of shear-stress partitioning predicts a low dependence on Γ. Consequently, it fails to explain the increase in slope ratio with Γ as observed in the Liwu River (Figure 10), and it can be generally ruled out in explaining any apparent trends of increase in slope ratio with boulder concentration. The prediction of the reduction in the transport efficiency model could explain the trend observed in the data (Figure 8), yet it requires the calibration of four parameters. Although, according to this model, in the general case, the slope ratio is a function of the width ratio, we find that the best-fit parameters are those that make the slope ratio independent of the width ratio. This outcome points to a steepening effect that relies solely on sediment entrainment and deposition to form a steeper bed and can occur very fast, probably within one or a few floods (Turowski, 2020). This mechanism differs from the one proposed by Shobe et al. (2020), which relied on bedrock erosion to induce steepening, and would therefore have a much longer adjustment timescale. The inferred independence of the slope ratio and the width ratio, manifested by the small q (power of the width ratio), reinforces our hypothesis of substantial difference in the adjustment timescales of bedrock width and sediment-bed slope. In other locations with much softer and erodible banks (e.g., Cook et al., 2014), a covariation of slope and width is hypothesized to be more significant. Whereas standard models commonly assume that q is either zero or one, it is also possible that the dependence of sediment flux on channel width is diminished in the long term, thus constraining q to be close to zero (Rickenmann, 2001). Further research on the value of q for different timescales of sediment transport is warranted. Given the good fit and the general agreement of the model with the data, we attribute most of the steepening of the boulder-bed channel reaches to a necessity to mobilize the upstream sediment supply despite the presence of large boulders that reduce the overall sediment transport efficiency.

The reduction in the transport efficiency model predicts a monotonic steepening effect with increasing boulder concentration. However, with increasing boulder concentration, we expect channel slope to decrease as the channel self-organizes a new bed largely composed of boulders such that boulders are no longer significant roughness elements on the bed. This situation is equivalent to the role of boulder spacing, shown by flume experiments, to strongly influence grade conditions (McKie et al., 2021). Each boulder generates a unique zone susceptible to flow reversals and enhanced turbulence (Papanicolaou & Tsakiris, 2017). However, when the spacing is small, the different boulder-influenced zones interact, causing an overall reduction in the total influence zone. Our developed equation does not show this behavior because of the assumption that the transport efficiency decreases monotonically for the entire range of Γ (Equation 19).

6.2. Reviewing the Assumptions of Steady-States

In our theoretical framework, we assumed several forms of steady-states, from which we derived equations relating channel morphology and boulder concentration. Among the examined models, some have performed better, while others showed a certain degree of incompatibility compared to the data (Section 5; Table 2), thus requiring an assessment of the applicability of the steady-state assumptions to the Liwu River.

Historical satellite images (Google Earth) from the early 21st century show that boulder patterns and quantities in the Liwu River resemble those of today. We assumed that boulder concentration is steady during the adjustment period of channel width and slope. This assumption may have different degrees of validity for the width and slope, due to their distinct adjustment timescales. As is supported by our findings, adjustment by channel steepening can occur rapidly by redistributing sediments throughout the fluvial reach. The rate at which a new sediment bed slope forms depends on various hydrological and morphological parameters, such as water discharge, shear stress, and the grain size of the mobile sediment (e.g., Barry et al., 2004). The Liwu River may be a locality in which large water discharge variability (Lague et al., 2005) and magnitude are expected to promote more sediment transport

events per given flood season (Dadson et al., 2003; Hartshorn et al., 2002). For example, observations from the Liwu River show it was able to remove (Lague, 2010) and deposit (Turowski et al., 2008) sediments a few meters in depth following a typhoon event. Theory suggests that sediment entrainment and deposition processes can occur within periods ranging from several days to a few tens of years (Turowski, 2020). Field evidence supports recognizing grade conditions in many bedrock river environments (Phillips & Jerolmack, 2016). Taken together, this evidence leads us to propose that boulder concentration is steady for periods larger than the slope adjustment timescale, reinforcing the plausible assumption that the Liwu River is close to grade.

In contrast to slope, channel widening results from lateral bedrock erosion, a process that can span thousands of years. This longer timescale calls for a more careful consideration of the rate at which boulder concentration varies, which depends on the boulder mass balance: its supply, transport, and breakdown. In numerous reaches that we examined, there is direct evidence for a continuous supply of large boulders (see Supporting Information S1). Hillslopes near boulder-bed channels often exhibit scars typical of landslides and rockfalls. However, whether those boulders were delivered to the Liwu River tributaries recently or if they were placed a long time ago requires further research. Field evidence from other tectonically active sites such as Himalayan rivers (Huber et al., 2020) and steep channels draining into the Dead-sea, Israel (Haviv, 2007), demonstrates that boulders may last in rivers for periods of tens of thousands of years.

Abrasion of boulders and other related bed obstacles in the Liwu River has been attributed predominantly to the impact of bedload particles (Wilson et al., 2013). The abrasion rates measured by Wilson et al. (2013) are very similar to the lateral erosion rates along the Liwu river (Hartshorn et al., 2002; Turowski et al., 2008). Thus, the rate at which channel width shapes seemingly resembles that of boulder abrasion. Ultimately, channel width in the Liwu River may be at a steady-state for uplift, sediment supply, and discharge. However, it is uncear whether width has completely adjusted to boulder input. To gain insights on steady-state channel morphology with regards to boulders, further research is needed to unravel boulder durability in fluvial environments.

6.3. Causality Between Boulder Concentration and Channel Width

The models proposed to explain the observed relation between boulder concentration and the width ratio assume that channel width adjusts (and is, therefore, the dependent variable) to boulder concentration. Notwithstanding, the causality between the two variables can also be presented inversely. Here we pose a hypothesis for a potential dependence of boulder concentration on channel width. Consider a case in which boulders have an equal probability of arriving at a specific location within the river and assume an initial variability in channel width along the river. In wider reaches, the fluid shear stress driving both bedload transport, which is responsible for boulder abrasion (Wilson et al., 2013), and boulder transportation is smaller relative to a narrow channel with otherwise the same parameters. Since bedload transport depends on discharge and erosion depends on bedload, boulders will both abrade and be transported quicker in narrower channels. In such a case, observations would be of a positive scaling of channel width with boulder concentration. However, if width is the independent variable, it can be expected to scale negatively with slope (Attal et al., 2008; Finnegan et al., 2005), yet such a scaling is not apparent in our data set (Figure S7 in Supporting Information S1).

7. Conclusions

Large, rarely mobile boulders hamper the hydrodynamics and sediment transport processes of bedrock channels. Boulder emplacement is a significant perturbation to the channel, which is expected to respond by changing its geometry. We developed mechanistic models for steady-state channel morphology in the presence of large boulders in bedrock channels. Rock and sediment mass balance principles were applied to explore possible processes that induce channel width and slope adjustment in response to boulder concentration. This theoretical framework yields analytic predictions for the width and slope ratios, defined as the ratio of boulder-bed to the equivalent boulder-free quantity. Under the first principle of rock mass balance, we assumed that boulder-bed and boulder-free reaches erode into bedrock at the same rate. We expanded this assumption by considering three effects that boulders impose on the process of bedrock erosion: the cover, the tools, and the multi-channel effect. These models yielded predictions for the width ratio as a function of boulder concentration. Under the second principle, we assumed that bedload flux in equivalent boulder-bed and boulder-free reaches is identical under equilibrated grade conditions. Here, two underlying mechanisms were examined for the effect of boulders on

bedload transport: a reduction in the efficiency of sediment mobilization and a reduction in the available shear stress for sediment mobilization. Both mechanisms yielded solutions for the slope ratio as a function of boulder concentration, while the second mechanism provided an independent solution to the width ratio.

The predictions of the different models were tested against newly collected data from the Liwu River, Taiwan, where numerous reaches exhibit a wide spectrum of boulder concentration, ranging from zero to 35%. The data show positive correlation between sediment-bed slope and bedrock width against boulder concentration. Following a normalization procedure, the correlation between the normalized width and boulder concentration improved but the width data remained relatively scattered. The normalized slope exhibits a pronounced positive scaling with boulder concentration.

The cover effect by boulders predicts that the width is independent of boulder concentration, in contrast to the widening trend in the data. The tools effect predicts a slight widening but the overall magnitude underpredicts the Liwu data. A shear-stress partitioning model can account for a fraction of the width data but requires information about several parameters, which we have not been able to independently constrain. Assuming that boulders split the flow into inner flows and sediments are equally distributed within those in-channels, a multi-channel effect captures a substantial fraction of the width variability. However, the reach geometry associated with this model is somewhat inconsistent with field observations. Generally, we interpret the scatter in width data and the inability of any of the proposed models to predict as an indication for the long timescale of channel width adjustment in response to boulder concentration. Consequently, different reaches have adjusted at different extents. However, we cannot rule out that there exist controlling parameters, which are yet to be identified and may collapse boulder-bed width data onto a single trend. The slope ratio was best captured by the effect of a reduction in sediment transport efficiency, with little to no dependence on channel width. In contrast, a shear-stress partitioning effect cannot explain the trend in the slope ratio.

The theoretical framework presented here constitutes a first attempt to examine and test various physical mechanisms controlling the relationship between bedrock channel morphology and large boulders. Two key research directions originate from this study. First, we have insufficient insights into the dynamics of bedload relating to sediment deflection in the vicinity of boulders. Many of our model predictions may improve or change when the controls on the deflection length scale are better understood. Second, revealing the residence time of boulders in bedrock channels is expected to advance understanding about the relative timescales of boulder residence and channel morphological adjustments.

Appendix A: Slope Solution to the Shear-Stress Partitioning Effect

Here we solve the equation of shear-stress partitioning (Section 3.2.2) for the slope ratio. First, from geometry and continuity, it follows that (Turowski, 2021)

$$2Q\left(\frac{\tau}{\rho g}\right) = \mathrm{QSW} - K_{\mathrm{V}} W^2 S^{\frac{1}{2}-\delta}\left(\frac{\tau}{\rho g}\right)^{1+\delta} \tag{A1}$$

For intermediate width, the term on the left-hand side of the equation can be neglected, and Equation A1 can be solved for channel width

$$W = (\rho g)^{\delta+1}\frac{Q S^{\delta+0.5}}{K_{\mathrm{V}}}\tau^{-(\delta+1)} \tag{A2}$$

For a boulder-bed channel, Equation A2 can be rewritten as

$$W_{\mathrm{b}} = (\rho g)^{\delta+1}\frac{Q {S_{\mathrm{b}}}^{\delta+0.5}}{K_{\mathrm{V}}}{\tau_{\mathrm{ST}}}^{-(\delta+1)} \tag{A3}$$

Dividing Equation A3 by Equation A2

$$\frac{W_{\mathrm{b}}}{W} = \left(\frac{S_{\mathrm{b}}}{S}\right)^{\delta+0.5}\left(\frac{\tau_{\mathrm{ST}}}{\tau}\right)^{-(\delta+1)} \tag{A4}$$

From Equation 26, it follows that

$$\frac{W_b}{W} = \left(\frac{\tau^*_{ST}}{\tau^*}\right)^{-3/2} \quad \text{(A5)}$$

Equating Equations A4 and A5 and solving for the slope ratio

$$\frac{S_b}{S} = \left(\frac{\tau_{ST}}{\tau}\right)^{\frac{\delta-0.5}{\delta+0.5}} \quad \text{(A6)}$$

Finally, Equation 25 is substituted into Equation A6 to yield a solution for the slope ratio as a function of boulder concentration (Equation 28).

Conflict of Interest

The authors declare no conflicts of interest relevant to this study.

Data Availability Statement

Data used for models evaluations can be found in Table 1. Raw DEMs, orthophotos, and channel reach boundaries can be found in Nativ et al. (2022) with the URL https://zenodo.org/record/6371224#.YjdBkOpByUk. Width and slope error methods and calculations can be found in the Supporting Information S1 file.

Acknowledgments
Wen-sheng Chen and Wen-Yen Chang are warmly thanked for supporting field logistics and permissions in Taroko National Park, Taiwan. We thank Jui-Ming Chang and Yu-Hsuan Yin for field assistance and fruitful discussions. We thank Tom Kaholi for field assistance and boulder digitization. Hagar Tevet and Guy Fisch are thanked for assisting in boulder digitization. Charles Shobe, Anne Voigtländer, and Joel Scheingross provided comments on an earlier version of the manuscript. Rebecca Hodge and Aaron Steelquist are thanked for constructive comments that greatly improved the quality of the manuscript. This research and R.N. were supported by the Israel Science Foundation (Grants 832/14 No. 562/19) and the NSF-BSF Foundation (Grant 2018619). R.N. is further supported by the Ben-Gurion University of the Negev "Hightech, Biotech & Chemotech" scholarship. Fieldwork was supported by GFZ. Open Access funding enabled and organized by Projekt DEAL.

References

Attal, M., Tucker, G. E., Whittaker, A. C., Cowie, P. A., & Roberts, G. P. (2008). Modelling fluvial incision and transient landscape evolution: Influence of dynamic Channel adjustment. *Journal of Geophysical Research*, *113*(F3), 1–16. https://doi.org/10.1029/2007JF000893

Auel, C., Albayrak, I., Sumi, T., & Boes, R. M. (2017). Sediment transport in high-speed flows over a fixed bed: 2. Particle impacts and abrasion prediction. *Earth Surface Processes and Landforms*, *42*(9), 1365–1383. https://doi.org/10.1002/esp.4128

Barry, J. J., Buffington, J. M., & King, J. G. (2004). A general power equation for predicting bed load transport rates in gravel bed rivers. *Water Resources Research*, *40*(10), 1–22. https://doi.org/10.1029/2004WR003190

Bathurst, J. C. (1996). Field measurement of boulder flow drag. *Journal of Hydraulic Engineering*, *122*(3), 167–169. https://doi.org/10.1061/(asce)0733-9429(1996)122:3(167)

Beer, A. R., Turowski, J. M., & Kirchner, J. W. (2017). Spatial patterns of erosion in a bedrock gorge. *Journal of Geophysical Research: Earth Surface*, *122*(1), 191–214. https://doi.org/10.1002/2016JF003850

Bennett, G. L., Miller, S. R., Roering, J. J., & Schmidt, D. A. (2016). Landslides, threshold slopes, and the survival of relict terrain in the wake of the Mendocino Triple Junction. *Geology*, *44*(5), 363–366. https://doi.org/10.1130/G37530.1

Bravo, R., Ortiz, P., & Luis Pérez-Aparicio, J. (2018). Analytical and discrete solutions for the incipient motion of ellipsoidal sediment particles. *Journal of Hydraulic Research*, *56*(1), 29–43. https://doi.org/10.1080/00221686.2017.1289263

Buffington, J. M., & Montgomery, D. R. (1997). A systematic analysis of eight decades of incipient motion studies, with special reference to gravel-bedded rivers. *Water Resources Research*, *33*(8), 1993–2029. https://doi.org/10.1029/97WR03138

Canovaro, F., Paris, E., & Solari, L. (2007). Effects of macro-scale bed roughness geometry on flow resistance. *Water Resources Research*, *43*(10), 1–17. https://doi.org/10.1029/2006WR005727

Carling, P. A., Hoffmann, M., & Blatter, A. (2002). Initial motion of boulders in bedrock channels. In *Ancient floods, modern hazards: Principles and applications of paleoflood hydrology* (Vol. 5, pp. 147–160). American Geophysical Union.

Chiari, M., Friedl, K., & Rickenmann, D. (2010). A one-dimensional bedload transport model for steep slopes. *Journal of Hydraulic Research*, *48*(2), 152–160. https://doi.org/10.1080/00221681003704087

Cook, K. L., Andermann, C., Gimbert, F., Adhikari, B. R., & Hovius, N. (2018). Glacial lake outburst floods as drivers of fluvial erosion in the Himalaya. *Science*, *57*(6410), 53–57. https://doi.org/10.1126/science.aat4981

Cook, K. L., Turowski, J. M., & Hovius, N. (2013). A demonstration of the importance of bedload transport for fluvial bedrock erosion and knickpoint propagation. *Earth Surface Processes and Landforms*, *38*(7), 683–695. https://doi.org/10.1002/esp.3313

Cook, K. L., Turowski, J. M., & Hovius, N. (2014). River gorge eradication by downstream sweep erosion. *Nature Geoscience*, *7*(9), 682–686. https://doi.org/10.1038/ngeo2224

Cook, K. L., Turowski, J. M., & Hovius, N. (2020). Width control on event-scale deposition and evacuation of sediment in bedrock-confined channels. *Earth Surface Processes and Landforms*, *45*(14), 3702–3713. https://doi.org/10.1002/esp.4993

Dadson, S. J., Hovius, N., Chen, H., Dade, W. B., Hsieh, M. L., Willett, S. D., et al. (2003). Links between erosion, runoff variability and seismicity in the Taiwan orogen. *Nature*, *426*(6967), 648–651. https://doi.org/10.1038/nature02150

Davis, W. M. (1902). Base level, grade and peneplain. *The Journal of Geology*, *10*(1), 77–111. https://doi.org/10.1086/620982

Dey, S. (2014). *Fluvial hydrodynamics: Hydrodynamic and sediment transport phenomena*. Springer.

Dey, S., Sarkar, S., Bose, S. K., Tait, S., & Castro-Orgaz, O. (2011). Wall-wake flows downstream of a sphere placed on a plane rough wall. *Journal of Hydraulic Engineering*, *137*(10), 1173–1189. https://doi.org/10.1061/(asce)hy.1943-7900.0000441

DiBiase, R. A., & Whipple, K. X. (2011). The influence of erosion thresholds and runoff variability on the relationships among topography, climate, and erosion rate. *Journal of Geophysical Research*, *116*(F4), 1–17. https://doi.org/10.1029/2011JF002095

DiBiase, R. A., Whipple, K. X., Heimsath, A. M., & Ouimet, W. B. (2010). Landscape form and millennial erosion rates in the San Gabriel Mountains, CA. *Earth and Planetary Science Letters*, *289*(1–2), 134–144. https://doi.org/10.1016/j.epsl.2009.10.036

Einstein, G. A., & Banks, R. B. (1950). Fluid resistance of composite roughness. *Transactions American Geophysical Union*, *31*(4), 603–610. https://doi.org/10.1029/tr031i004p00603

Einstein, H. A. (1950). *The bed-load function for sediment transportation in open channel flows* (Vol. 1026). USDA, Soil Conservation Service Technical Bulletins.

Exner, F. M. (1925). Über die wechselwirkung zwischen wasser und geschiebe in flüssen. *Akademie der Wissenschaften in Wien, Mathematisch-NaturwissenschaftlicheKlasse*, *134*, 165–204.

Fernandez Luque, R., & Van Beek, R. (1976). Erosion and transport of bed-load sediment. *Journal of Hydraulic Research*, *14*(2), 127–144. https://doi.org/10.1080/00221687609499677

Finnegan, N. J., Broudy, K. N., Nereson, A. L., Roering, J. J., Handwerger, A. L., & Bennett, G. (2019). River channel width controls blocking by slow-moving landslides in California's Franciscan mélange. *Earth Surface Dynamics*, *7*(3), 879–894. https://doi.org/10.5194/esurf-7-879-2019

Finnegan, N. J., Roe, G., Montgomery, D. R., & Hallet, B. (2005). Controls on the channel width of rivers: Implications for modeling fluvial incision of bedrock. *Geology*, *33*(3), 229–232. https://doi.org/10.1130/G21171.1

Fuller, T. K., Gran, K. B., Sklar, L. S., & Paola, C. (2016). Lateral erosion in an experimental bedrock channel: The influence of bed roughness on erosion by bed load impacts. *Journal of Geophysical Research: Earth Surface*, *121*(5), 1081–1105. https://doi.org/10.1002/2014JF003086

Gilbert, G. K. (1877). *Report on the geology of the Henry Mountains*. US Government Printing Office.

Hartshorn, K., Hovius, N., Dade, W. B., & Slingerland, R. L. (2002). Climate-driven bedrock incision in an active mountain belt. *Science*, *297*(5589), 2036–2038. https://doi.org/10.1126/science.1075078

Haviv, I. (2007). Mechanics, morphology and evolution of vertical knickpoints (waterfalls) along the bedrock channels of the Dead Sea western tectonic escarpment. Ph.D. Thesis, The Hebrew University of Jerusalem Israel.

He, C., Yang, C., & Turowski, J. M. (2021). The effect of roughness spacing and size on lateral deflection of bedload particles. *Water Resources Research*, *57*(10). https://doi.org/10.1029/2021wr029717

Hovius, N., Stark, C. P., Hao-Tsu, C., & Jiun-Chuan, L. (2000). Supply and removal of sediment in a landslide-dominated mountain belt: Central range, Taiwan. *The Journal of Geology*, *108*(1), 73–89. https://doi.org/10.1086/314387

Huber, M. L., Lupker, M., Gallen, S. F., Christl, M., & Gajurel, A. P. (2020). Timing of exotic, far-traveled boulder emplacement and paleo-outburst flooding in the central Himalayas. *Earth Surface Dynamics*, *8*(3), 769–787. https://doi.org/10.5194/esurf-8-769-2020

Johnson, J. P. L., Whipple, K. X., & Sklar, L. S. (2010). *Contrasting Bedrock incision rates from snowmelt and flash floods in the Henry Mountains, Utah* (Vol. 122, pp. 1600–1615). Bulletin of the Geological Society of America. https://doi.org/10.1130/B30126.1

Johnson, J. P. L., Whipple, K. X., Sklar, L. S., & Hanks, T. C. (2009). Transport slopes, sediment cover, and bedrock channel incision in the Henry Mountains, Utah. *Journal of Geophysical Research*, *114*(F2), 1–21. https://doi.org/10.1029/2007JF000862

Jouvet, G., Seguinot, J., Ivy-Ochs, S., & Funk, M. (2017). Modelling the diversion of erratic boulders by the Valais Glacier during the last glacial maximum. *Journal of Glaciology*, *63*(239), 487–498. https://doi.org/10.1017/jog.2017.7

Lague, D. (2010). Reduction of long-term bedrock incision efficiency by short-term alluvial cover intermittency. *Journal of Geophysical Research*, *115*(F2). https://doi.org/10.1029/2008JF001210

Lague, D., Hovius, N., & Davy, P. (2005). Discharge, discharge variability, and the bedrock channel profile. *Journal of Geophysical Research*, *110*(F4), 1–17. https://doi.org/10.1029/2004JF000259

Lamb, M. P., Dietrich, W. E., & Venditti, J. G. (2008). Is the critical Shields stress for incipient sediment motion dependent on channel-bed slope. *Journal of Geophysical Research*, *113*(F2), 1–20. https://doi.org/10.1029/2007JF000831

Lenzi, M. A. (2001). Step-pool evolution in the Rio Cordon. *Northeastern Italy: Earth Surface Processes and Landforms*, *26*(9), 991–1008. https://doi.org/10.1002/esp.239

Li, T., Fuller, T. K., Sklar, L. S., Gran, K. B., & Venditti, J. G. (2020). A mechanistic model for lateral erosion of bedrock channel banks by bedload particle impacts. *Journal of Geophysical Research: Earth Surface*, *125*(6). https://doi.org/10.1029/2019JF005509

Mackin, J. H. (1948). Concept of the graded river. *The Geological Society of America Bulletin*, *59*(5), 463–512. https://doi.org/10.1130/0016-7606(1948)59[463:COTGR]2.0.CO;2

McKie, C. W., Juez, C., Plumb, B. D., Annable, W. K., & Franca, M. J. (2021). How large immobile sediments in gravel bed rivers impact sediment transport and bed morphology. *Journal of Hydraulic Engineering*, *147*(2), 04020096. https://doi.org/10.1061/(asce)hy.1943-7900.0001842

Meyer-Peter, E., & Müller, R. (1948). *Formulas for bed-load transport* (pp. 39–64). Proceedings of the 2nd meeting of the International Association of Hydraulic Research.

Montgomery, D. R., & Buffington, J. M. (1997). Channel-reach morphology in mountain drainage basins. *Bulletin of the Geological Society of America*, *109*, 596–611. https://doi.org/10.1130/0016-7606(1997)109<0596:CRMIMD>2.3.CO;2

Montgomery, D. R., & Gran, K. B. (2001). Downstream variations in the width of bedrock channels. *Water Resources Research*, *37*(6), 1841–1846. https://doi.org/10.1029/2000wr900393

Nativ, R., Turowski, J. M., Goren, L., Laronne, J. B., & Shyu, J. B. H. (2022). Influence of boulders on channel width and slope: Theory and Field Application. [Dataset]. Zenodo. https://doi.org/10.5281/zenodo.6371224

Nitsche, M., Rickenmann, D., Turowski, J. M., Badoux, A., & Kirchner, J. W. (2011). Evaluation of bedload transport predictions using flow resistance equations to account for macro-roughness in steep mountain streams. *Water Resources Research*, *47*(8). https://doi.org/10.1029/2011WR010645

Pagliara, S., & Chiavaccini, P. (2006). Flow resistance of rock chutes with protruding boulders. *Journal of Hydraulic Engineering*, *132*(6), 545–552. https://doi.org/10.1061/(ASCE)0733-9429

Papanicolaou, A. N., & Kramer, C. (2006). The role of relative submergence on cluster microtopography and bedload predictions in mountain streams: River, Coastal and Estuarine Morphodynamics: RCEM 2005. In *Proceedings of the 4th IAHR Symposium on River. Coastal and Estuarine Morphodynamics* (Vol. *2*, pp. 1083–1086). https://doi.org/10.1201/9781439833896.ch117

Papanicolaou, A. N., Kramer, C. M., Tsakiris, A. G., Stoesser, T., Bomminayuni, S., & Chen, Z. (2012). Effects of a fully submerged boulder within a boulder array on the mean and turbulent flow fields: Implications to bedload transport. *Acta Geophysica*, *60*(6), 1502–1546. https://doi.org/10.2478/s11600-012-0044-6

Papanicolaou, A. N., & Tsakiris, A. G. (2017). Boulder effects on turbulence and bedload transport. In D. Tsutsumi & J. B. Laronne (Eds.) *Gravel-Bed Rivers* (pp. 33–72). John Wiley & Sons Ltd. https://doi.org/10.1002/9781118971437.ch2

Papanicolaou, A. N. T., Tsakiris, A. G., Wyssmann, M. A., & Kramer, C. M. (2018). Boulder array effects on bedload pulses and depositional patches. *Journal of Geophysical Research: Earth Surface*, *123*(11), 2925–2953. https://doi.org/10.1029/2018JF004753

Phillips, C. B., & Jerolmack, D. J. (2016). Self-organization of river channels as a critical filter on climate signals. *Science*, *352*(6286), 694–697. https://doi.org/10.1126/science.aad3348

Polvi, L. E. (2021). Morphodynamics of boulder-bed semi-alluvial streams in northern Fennoscandia: A flume experiment to determine sediment self-organization. *Water Resources Research*, *57*(3). https://doi.org/10.1029/2020WR028859

Prancevic, J. P., & Lamb, M. P. (2015). Unraveling bed slope from relative roughness in initial sediment motion. *Journal of Geophysical Research: Earth Surface*, *120*(3), 474–489. https://doi.org/10.1002/2014JF003323.Received

Rickenmann, D. (2001). Comparison of bed load transport in torrents and gravel bed streams. *Water Resources Research*, *37*(12), 3295–3305. https://doi.org/10.1029/2001wr000319

Royden, L., & Perron, J. T. (2013). Solutions of the stream power equation and application to the evolution of river longitudinal profiles. *Journal of Geophysical Research: Earth Surface*, *118*(2), 497–518. https://doi.org/10.1002/jgrf.20031

Schneider, J. M., Rickenmann, D., Turowski, J. M., Bunte, K., & Kirchner, J. W. (2015). Applicability of bed load transport models for mixed-size sediments in steep streams considering macro-roughness. *Water Resources Research*, *51*(7), 5260–5283. https://doi.org/10.1002/2014WR016417

Schneider, J. M., Rickenmann, D., Turowski, J. M., & Kirchner, J. W. (2015). Self-adjustment of stream bed roughness and flow velocity in a steep mountain channel. *Water Resources Research*, *51*(10), 7839–7859. https://doi.org/10.1002/2015WR016934

Schumm, S. A., & Parker, R. S. (1973). Implications of complex response of drainage systems for Quaternary alluvial stratigraphy. *Nature; Physical Science*, *243*(128), 99–100. https://doi.org/10.1038/physci243099a0

Seizilles, G., Lajeunesse, E., Devauchelle, O., & Bak, M. (2014). Cross-stream diffusion in bedload transport. *Physics of Fluids*, *26*(1), 013302. https://doi.org/10.1063/1.4861001

Shobe, C. M., Bennett, G. L., Tucker, G. E., Roback, K., Miller, S. R., & Roering, J. J. (2020). *Boulders as a lithologic control on river and landscape response to tectonic forcing at the Mendocino triple junction* (pp. 1–16). Geological Society of America Bulletin. https://doi.org/10.1130/B35385.1

Shobe, C. M., Tucker, G. E., & Anderson, R. S. (2016). Hillslope-derived blocks retard river incision. *Geophysical Research Letters*, *43*(10), 5070–5078. https://doi.org/10.1002/2016GL069262.1

Shobe, C. M., Tucker, G. E., & Rossi, M. W. (2018). Variable-threshold behavior in rivers arising from hillslope-derived blocks. *Journal of Geophysical Research: Earth Surface*, *123*(8), 1–27. https://doi.org/10.1029/2017JF004575

Shobe, C. M., Turowski, J. M., Nativ, R., Glade, R. C., Bennett, G. L., & Dini, B. (2021). The role of infrequently mobile boulders in modulating landscape evolution and geomorphic hazards. *Earth-Science Reviews*, *220*, 103717. https://doi.org/10.1016/j.earscirev.2021.103717

Sklar, L., & Dietrich, W. E. (1998). River longitudinal profiles and bedrock incision models: Stream power and the influence of sediment supply. In K. J. Tinkler & E. Wohl (Eds.) *Rivers over rock: Fluvial processes in bedrock channels, geophysical monograph series* (Vol. *107*, pp. 237–260). https://doi.org/10.1029/GM107

Sklar, L. S., & Dietrich, W. E. (2004). A mechanistic model for river incision into bedrock by saltating bed load. *Water Resources Research*, *40*(6), 1–22. https://doi.org/10.1029/2003WR002496

Sklar, L. S., & Dietrich, W. E. (2006). The role of sediment in controlling steady-state bedrock channel slope: Implications of the saltation-abrasion incision model. *Geomorphology*, *82*(1–2), 58–83. https://doi.org/10.1016/j.geomorph.2005.08.019

Teng, L. S. (1990). Geotectonic evolution of late Cenozoic arc-continent collision in Taiwan. *Tectonophysics*, *183*(1–4), 57–76. https://doi.org/10.1016/0040-1951(90)90188-E

Thaler, E. A., & Covington, M. D. (2016). The influence of sandstone caprock material on bedrock channel steepness within a tectonically passive setting: Buffalo National River Basin, Arkansas, USA. *Journal of Geophysical Research: Earth Surface*, *121*(9), 1635–1650. https://doi.org/10.1002/2015JF003771

Tsakiris, A. G., Papanicolaou, A. N. T., Hajimirzaie, S. M., & Buchholz, J. H. J. (2014). Influence of collective boulder array on the surrounding time-averaged and turbulent flow fields. *Journal of Mountain Science*, *11*(6), 1420–1428. https://doi.org/10.1007/s11629-014-3055-8

Turowski, J. M. (2018). Alluvial cover controlling the width, slope and sinuosity of bedrock channels. *Earth Surface Dynamics*, *6*(1), 29–48. https://doi.org/10.5194/esurf-6-29-2018

Turowski, J. M. (2020). Mass balance, grade, and adjustment timescales in bedrock channels. *Earth Surface Dynamics*, *8*(1), 103–122. https://doi.org/10.5194/esurf-2019-47

Turowski, J. M. (2021). Upscaling sediment-flux-dependent fluvial bedrock incision to long timescales. *Journal of Geophysical Research: Earth Surface*, *126*(5). https://doi.org/10.1029/2020jf005880

Turowski, J. M., & Hodge, R. (2017). A probabilistic framework for the cover effect in bedrock erosion. *Earth Surface Dynamics*, *5*(2), 311–330. https://doi.org/10.5194/esurf-5-311-2017

Turowski, J. M., Hovius, N., Lague, D., Hsieh, M.-L., & Men-Chiang, C. (2008). Distribution of erosion across bedrock channels. *Earth Surface Processes and Landforms*, *33*(3), 353–363. https://doi.org/10.1002/esp.1559

Turowski, J. M., Lague, D., & Hovius, N. (2007). Cover effect in bedrock abrasion: A new derivation and its implications for the modeling of bedrock channel morphology. *Journal of Geophysical Research*, *112*(F4), 1–16. https://doi.org/10.1029/2006JF000697

Turowski, J. M., Lague, D., & Hovius, N. (2009). Response of bedrock channel width to tectonic forcing: Insights from a numerical model, theoretical considerations, and comparison with field data. *Journal of Geophysical Research*, *114*(F3), 1–16. https://doi.org/10.1029/2008JF001133

Turowski, J. M., Yager, E. M., Badoux, A., Rickenmann, D., & Molnar, P. (2009). The impact of exceptional events on erosion, bedload transport and channel stability in a step-pool channel. *Earth Surface Processes and Landforms*, *34*(12), 155–161. https://doi.org/10.1002/esp

Westoby, M. J., Brasington, J., Glasser, N. F., Hambrey, M. J., & Reynolds, J. M. (2012). "Structure-from-Motion" photogrammetry: A low-cost, effective tool for geoscience applications. *Geomorphology*, *179*, 300–314. https://doi.org/10.1016/j.geomorph.2012.08.021

Whipple, K. X. (2004). Bedrock rivers and the geomorphology of active orogens. *Annual Review of Earth and Planetary Sciences*, *32*(1), 151–185. https://doi.org/10.1146/annurev.earth.32.101802.120356

Whipple, K. X., & Tucker, G. E. (1999). Dynamics of the stream-power river incision model: Implications for height limits of mountain ranges, landscape response timescales, and research needs. *Journal of Geophysical Research*, *104*(B8), 17661–17674. https://doi.org/10.1029/1999JB900120

Whitbread, K., Jansen, J., Bishop, P., & Attal, M. (2015). Substrate, sediment, and slope controls on bedrock channel geometry in postglacial streams. *Journal of Geophysical Research: Earth Surface*, *120*(5), 779–798. https://doi.org/10.1002/2014JF003295

Wiberg, P. L., & Smith, J. D. (1991). Velocity distribution and bed roughness in high-gradient streams. *Water Resources Research*, *27*(5), 825–838. https://doi.org/10.1029/90WR02770

Wilson, A., Hovius, N., & Turowski, J. M. (2013). Geomorphology Upstream-facing convex surfaces: Bedrock bedforms produced by fluvial bedload abrasion. *Geomorphology*, *180–181*, 187–204. https://doi.org/10.1016/j.geomorph.2012.10.010

Wobus, C., Whipple, K. X., Kirby, E., Snyder, N., Johnson, J., Spyropolou, K., et al. (2006). *Tectonics from topography: Procedures, promise, and pitfalls* (Vol. 398, pp. 55–74). Geological Society of America. https://doi.org/10.1130/2006.2398(04)

Wong, M., & Parker, G. (2006). Reanalysis and correction of bed-load relation of Meyer-Peter and Müller using their own database. *Journal of Hydraulic Engineering*, *132*(11), 1159–1168. https://doi.org/10.1061/(ASCE)0733-9429

Yager, E. M., Kirchner, J. W., & Dietrich, W. E. (2007). Calculating bed load transport in steep boulder bed channels. *Water Resources Research*, *43*(7), 1–24. https://doi.org/10.1029/2006WR005432

Yanites, B. J. (2018). The dynamics of channel slope, width, and sediment in actively eroding bedrock river systems. *Journal of Geophysical Research: Earth Surface*, *123*(7), 1504–1527. https://doi.org/10.1029/2017JF004405